

# Systematic uncertainties from halo asphericity in dark matter searches

Nicolás Bernal,<sup>1</sup> Jaime E. Forero-Romero,<sup>2</sup> Raghuvveer Garani<sup>3</sup>  
and Sergio Palomares-Ruiz<sup>4</sup>

<sup>1</sup>ICTP South American Institute for Fundamental Research, Instituto de Física Teórica, Universidade Estadual Paulista, São Paulo, Brazil

<sup>2</sup>Departamento de Física, Universidad de los Andes, Cra. 1 No. 18A-10, Edificio Ip, Bogotá, Colombia

<sup>3</sup>Bethe Center for Theoretical Physics and Physikalisches Institut, Universität Bonn, Nußallee 12, D-53115 Bonn, Germany

<sup>4</sup>Instituto de Física Corpuscular (IFIC), CSIC-Universitat de València, Apartado de Correos 22085, E-46071 València, Spain

E-mail: [nicolas@ift.unesp.br](mailto:nicolas@ift.unesp.br), [je.forero@uniandes.edu.co](mailto:je.forero@uniandes.edu.co),  
[garani@th.physik.uni-bonn.de](mailto:garani@th.physik.uni-bonn.de), [sergio.palomares.ruiz@ific.uv.es](mailto:sergio.palomares.ruiz@ific.uv.es)

**Abstract.** Although commonly assumed to be spherical, dark matter halos are predicted to be non-spherical by N-body simulations and their asphericity has a potential impact on the systematic uncertainties in dark matter searches. The evaluation of these uncertainties is the main aim of this work, where we study the impact of aspherical dark matter density distributions in Milky-Way-like halos on direct and indirect searches. Using data from the large N-body cosmological simulation Bolshoi, we perform a statistical analysis and quantify the systematic uncertainties on the determination of local dark matter density and the so-called  $J$  factors for dark matter annihilations and decays from the galactic center. We find that, due to our ignorance about the extent of the non-sphericity of the Milky Way dark matter halo, systematic uncertainties can be as large as 35%, within the 95% most probable region, for a spherically averaged value for the local density of 0.3-0.4 GeV/cm<sup>3</sup>. Similarly, systematic uncertainties on the  $J$  factors evaluated around the galactic center can be as large as 10% and 15%, within the 95% most probable region, for dark matter annihilations and decays, respectively.

---

## Contents

<b>1</b>	<b>Introduction</b>	<b>1</b>
<b>2</b>	<b>Direct and indirect dark matter searches</b>	<b>3</b>
<b>3</b>	<b>Simulations</b>	<b>4</b>
3.1	Halo finding	4
3.2	Shape parameter	5
3.3	Concentration parameter	5
3.4	Data set	7
<b>4</b>	<b>Impact of halo asphericity</b>	<b>8</b>
<b>5</b>	<b>Observational priors</b>	<b>11</b>
5.1	The virial mass of the Milky Way	11
5.2	The mass of the Milky Way within 60 kpc	12
5.3	Local dark matter surface density	13
5.4	Sun’s galactocentric distance	13
<b>6</b>	<b>Results</b>	<b>14</b>
6.1	Systematic uncertainties on $\rho_{\odot}$	14
6.2	Systematic uncertainties on $\bar{J}_{\text{ann}}$ and $\bar{J}_{\text{dec}}$	16
<b>7</b>	<b>Discussion and Conclusions</b>	<b>19</b>

---

## 1 Introduction

Detecting and constraining the nature of dark matter (DM) is one of the most pressing issues in physics today. In contrast to collider DM searches, direct and indirect detection methods crucially depend on the properties of the DM halo of the Milky Way. The number of nuclear recoil events in direct detection experiments depends on the flux of DM particles through the detector, which in turn depends on the local DM density. Searches for neutrinos from DM annihilations in the Sun or Earth depend on the capture rate of DM particles, which also depends on the flux of DM particles in the solar neighborhood, hence, on the local DM density. In addition, the flux of gamma-rays and neutrinos produced in DM annihilations or decays in the galaxy depends on the shape and orientation of the DM halo in the direction of observation.

Most mass models of the Milky Way decompose the galaxy into three components (the bulge, the disc and the dark halo), which are usually described using analytical models constrained from observational data, such as terminal velocities in the inner galaxy, rotation velocities in the outer galaxy, the solar position and velocity, the Oort’s constants, the mass at large radii, the local surface density, etc. [1–6]. The observational constraints for the local DM density are of two types. Some constraints are truly local and are derived from stellar dynamics, whereas others are constraints over an spherical average of the rotation curve. These two values are expected to be different in the case of a triaxial DM halo, but most of the models of the galaxy have spherical symmetry.

However, it is well known that N-body simulations predict halos to be triaxial, being close to prolate in the inner part and rounder at larger distances from the center [7–25], although with the incorporation of baryons they predict halos to become rounder [26–30]. Observationally, early dynamical studies using stellar kinematics and the variation in thickness of the Milky Way’s HI layer with radius, concluded that the DM halo around the galactic disk is oblate [31]. On the other hand, in the Milky Way, the gravitational potential can be constrained by using tidal streams of stars located at large distances from the galactic center, where the potential is dominated by the DM component. This latter approach has been followed in recent years by using the Sagittarius dwarf tidal stream [32–42]. However, very different conclusions have been reached depending on the adopted criterion. An almost spherical halo was found in early works [32, 36], whereas an oblate halo has also been claimed [34, 37–40, 42], and even a prolate halo has been suggested [33]. The triaxiality of the halo was required in order to simultaneously fit the density profile and the kinematics of the stream [38–40]. However, this almost oblate ellipsoid was found to have the minor axis contained within the galactic disc, which represents an unstable configuration [43]. In addition, it has been recently suggested that spherical solutions should be also allowed by observational data [41]. Thus, the debate about the shape and configuration of the DM halo of the Milky Way is open and a final consensus is far from being reached. Therefore, in this paper we do not use any observational constraint on the degree of triaxiality of the Milky Way DM halo.

The effects of triaxiality on the estimates for the local DM density have been studied in Ref. [44], using a simulation with only DM, and in Ref. [45], with simulations of two Milky-Way-like galaxies including baryons. In the DM-only simulation, a maximum total spread of a factor of  $\pm 2$  with a standard deviation  $\sigma(\bar{\rho})/\bar{\rho} \approx 0.26$  at 8 kpc from the galactic center was found [44]. With the inclusion of baryons, it was concluded that halo asphericity could lead up to 41% overdensity at the local distance with respect to the spherically averaged value [45]. The impact of halo asphericity on the so-called  $J$  factors in indirect searches is briefly discussed in Ref. [46].

In this work, we present an analysis based on a sample of  $\sim 10^5$  DM-only halos from the **Bolshoi** simulation [47]. The selected halos are compatible with the mass range of the Milky Way. Using this sample we construct the probability distributions of the parameters that define the density profile. The goal of this work is to study the impact of our lack of knowledge about the triaxial nature of the Milky Way DM halo on both direct and indirect searches of DM and hence, to estimate the amplitude of the systematic uncertainties originating from the halo asphericity in the determination of the local DM density and on the  $J$  factors.

The outline of the paper is as follows. In Sec. 2 we emphasize the dependence of direct and indirect DM detection searches on the local DM density and on the  $J$  factors. In Sec. 3, we discuss the data set we select from the **Bolshoi** simulation and the parametrization of the triaxial density profile for all the halos. In Sec. 4, we use three examples to illustrate the impact of halo asphericity on the departure of the local DM density and  $J$  factors from their respective spherically averaged values. In Sec. 5, we describe the different observational constraints we consider. In Sec. 6, using the whole data set of halos, we present our results for the overall probability distributions of the deviations from the spherical averages and discuss the uncertainties owing to triaxiality on the local DM density and the  $J$  factors. Finally, Sec. 7 is devoted to the discussion of our results and to the conclusion.

## 2 Direct and indirect DM searches

Direct detection experiments are designed to detect DM particles through their scattering with the nuclei in the detector, by measuring low energy nuclear recoils. The rate of such events are proportional to the flux of DM particles streaming through the surface of the Earth, which is in turn proportional to the local DM density,  $\rho_\odot$ . Qualitatively, the event rate  $R$  is given by [48]

$$R \approx \frac{\rho_\odot \sigma \langle v \rangle}{m_\chi m_A}, \quad (2.1)$$

where  $\sigma$  is the scattering cross section,  $\langle v \rangle$  is the average relative speed of DM with respect to the target,  $m_\chi$  is the DM mass and  $m_A$  is the mass of the target nuclei. Thus, when measuring recoil rates, the local DM density is fully correlated with the scattering cross section. Hence, accurate determination of the local DM density is crucial to constraint particle physics models.

In addition to direct searches, the local DM density is of key importance in estimating the number of neutrino events from DM annihilations accumulated in the Sun. The flux of neutrinos at the detectors on Earth is proportional to the annihilation rate of DM particles in the Sun, which is proportional to the Sun's capture rate of DM particles, which in turn is proportional to the flux of DM particles through the Sun, and hence it is proportional to the local DM density.

There are two methods to estimate the value of the local DM density. Either by constructing three-component (disc, bulge and dark halo) models for the galaxy and confronting them against observational data [49], or by calculating the DM density locally from the stellar kinematics in our neighborhood [50–53]. The analyses of the first type assume axisymmetric components and the value of  $\rho_\odot$  obtained from them actually refers to the spherically averaged density  $\langle \rho_\odot \rangle$ . The value that has been usually assumed, within an uncertainty of a factor of two, is  $\langle \rho_\odot \rangle \simeq 0.3 \text{ GeV/cm}^3$ . Several recent analyses have been performed using new data. Some of them model the galaxy and use a large and new set of observational constraints of the Milky Way [3–6, 54–56], whereas in Ref. [57] no modeling of the galaxy was needed.

Studies of the kinematics of stars around the Sun have also provided recent estimates, which are in general in agreement with the previous studies [58–62], although with larger errors. Some of these works have even suggested a local DM density as large as  $\sim 1 \text{ GeV/cm}^3$  [63, 64]. A thorough review of all the local DM density measurements can be found in Ref. [65], where a compilation of data from the literature is presented and values for the spherical estimates are found to fall into the range  $\sim 0.2\text{--}0.6 \text{ GeV/cm}^3$ .

As for indirect detection of DM annihilations or decays from the galactic center, the halo shape is also important. This can be seen as follows. The differential flux of prompt gamma-rays and neutrinos generated from DM annihilations (decays) in the smooth Milky Way DM halo after the hadronization, fragmentation and decay of the final states and coming from a direction within a solid angle  $\Delta\Omega$ , can be written as [66]

$$\begin{aligned} \frac{d\Phi_{\text{ann}}}{dE}(E, \Delta\Omega) &= \frac{\langle \sigma v \rangle}{2 m_\chi^2} \sum_i \text{BR}_i \frac{dN_{\text{ann}}^i}{dE} \bar{J}_{\text{ann}}(\Omega) \frac{\Delta\Omega}{4\pi}, \\ \frac{d\Phi_{\text{dec}}}{dE}(E, \Delta\Omega) &= \frac{1}{m_\chi \tau_\chi} \sum_i \text{BR}_i \frac{dN_{\text{dec}}^i}{dE} \bar{J}_{\text{dec}}(\Omega) \frac{\Delta\Omega}{4\pi}, \end{aligned} \quad (2.2)$$

where  $\langle \sigma v \rangle$  is the thermal average of the total DM annihilation cross section times the relative velocity,  $\tau_\chi$  is the DM lifetime, the discrete sum is over all DM annihilation (decay) channels,

$BR_i$  is the branching ratio of DM annihilation (decay) into the  $i$ -th final state and  $dN_{\text{ann}}^i/dE$  ( $dN_{\text{dec}}^i/dE$ ) is the differential gamma-ray or neutrino spectrum for the  $i$ -th channel. The quantities  $\bar{J}_{\text{ann}}(\Omega)$  and  $\bar{J}_{\text{dec}}(\Omega)$ , which depend crucially on the DM distribution are defined as

$$\begin{aligned}\bar{J}_{\text{ann}}(\Omega) &= \frac{1}{\Delta\Omega} \int_{\Delta\Omega} d\Omega \int_{\text{los}} \rho(r(s, \Omega))^2 ds , \\ \bar{J}_{\text{dec}}(\Omega) &= \frac{1}{\Delta\Omega} \int_{\Delta\Omega} d\Omega \int_{\text{los}} \rho(r(s, \Omega)) ds ,\end{aligned}\tag{2.3}$$

where the spatial integration of  $\rho(r)^2$  and  $\rho(r)$  is performed along the line of sight within the solid angle of observation  $\Delta\Omega$ . Let us stress that for DM annihilations, the  $J$  factor depends on the square of the DM density, whereas for decays it depends linearly on the DM density. Therefore, these quantities depend, not only on the local DM density, but also on the shape of the halo in the direction of observation. Indeed, gamma-ray observations could, in turn, be used to constrain the density profile [67–74].

### 3 Simulations

We use the results obtained from a large N-body cosmological simulation dubbed **Bolshoi** [47]. The data used in this work is publicly available through the *MultiDark Database*<sup>1</sup> presented by Ref. [75]. The **Bolshoi** simulation follows the non-linear evolution of DM density fluctuations in a cubic volume of length  $250h^{-1}\text{Mpc}$  sampled with  $2048^3$  particles. The Adaptive Refinement Tree (ART) code was used [76] and a detailed description of this simulation can be found in Ref. [47].

The cosmological parameters in this simulation are compatible with the results from the ninth year data releases from the Wilkinson Microwave Anisotropy Probe [77], with  $\Omega_m = 0.27$ ,  $\Omega_\Lambda = 0.73$ ,  $n_s = 0.95$ ,  $h = 0.70$  and  $\sigma_8 = 0.82$  for the matter density, dark energy density, slope of the matter fluctuations, the Hubble constant at  $z = 0$  in units of  $100 \text{ km s}^{-1} \text{ Mpc}^{-1}$  and the normalization of the power spectrum, respectively. With these parameters the mass of a simulation particle is  $m_p = 1.4 \times 10^8 h^{-1} M_\odot$ .

#### 3.1 Halo finding

We use halos that were defined using the Bound Density Maxima (BDM) algorithm [78]. The first step in the algorithm is finding the density at the positions of the particles in the simulation using a top-hat filter with typically 20 particles. After finding all maxima, halos are defined as the spheres of radius  $r_\Delta$  (centered around the maxima) which contain an overdensity mass  $M_\Delta = \frac{4\pi}{3} \Delta \rho_c(z) r_\Delta^3$ , where  $\rho_c(z)$  is the critical density of the Universe at redshift  $z$  and  $\Delta$  is a given overdensity, with [79]

$$\begin{aligned}M_v &= \frac{4\pi}{3} \Delta_v \rho_c(z) r_v^3 , \\ \Delta_v &= 18\pi^2 + 82(\Omega_m(z) - 1) - 39(\Omega_m(z) - 1)^2 .\end{aligned}\tag{3.1}$$

Let us note that there are a few cases where the halo is truncated to have a radius smaller than  $r_v$ . These few cases correspond to halos that are about to merge with other massive structures, so the radius corresponds to the distance to the surface where the density

<sup>1</sup><http://www.multidark.org/MultiDark/MyDB>

raises again due to the proximity to the soon-to-be host halo. The particles in the halo are also subject to an unbinding process, whereby the kinetic energy of each particle is compared against the gravitational potential. Particles that are found to be gravitational unbound are removed from the halo.

### 3.2 Shape parameter

In order to model halos as ellipsoids, the axis ratios and orientation is obtained by diagonalizing the shape tensor (see Ref. [80] for a critical discussion of different definitions), computed from all the bound particles inside the halo radius,

$$S_{ij} = \sum_n \frac{x_{i,n}x_{j,n}}{r_n^2}, \quad (3.2)$$

where  $x_{i,n}$  is the  $i$ -th Cartesian coordinate and  $r_n$  is the radial coordinate of the  $n$ -th particle in the halo, respectively. The eigenvalues of this tensor determine the length of the axes,  $a \geq b \geq c$ , and its eigenvectors determine the orientation of the halo. The axes ratios,  $b/a$  and  $c/a$ , correspond to ratios of eigenvalues.

The algorithm does not include any correction due to the fact that  $S_{ij}$  is calculated on a spherical region. However we apply such a correction, which depends on the halo concentration, being smaller for more concentrated halos. Defining  $\gamma = r_{\text{rms}}/r_v$ , where  $r_{\text{rms}} = \sqrt{\sum_n m_n r_n^2 / \sum_n m_n}$ , the true axial ratios are computed using the following formulae [75]:

$$\left(\frac{c}{a}\right)_{\text{true}} = \left(\frac{c}{a}\right)^{\alpha}, \quad \alpha = 1 + 2 \max[\gamma - 0.4, 0] + (5.5 \max[\gamma - 0.4, 0])^3, \quad (3.3)$$

$$\left(\frac{b}{a}\right)_{\text{true}} = \left(\frac{b}{a}\right)^{\beta}, \quad \beta = 1 + 2 \max[\gamma - 0.4, 0] + (5.7 \max[\gamma - 0.4, 0])^3. \quad (3.4)$$

These relationships were calibrated against the results of a more computationally expensive algorithm for measuring halo shapes [16]. This method starts from the spherical analysis provided by the BDM algorithm, then, ellipsoidal boundaries and orientation is redefined in accordance to the determined values of  $b/a$  and  $c/a$ , as described above; by keeping the longest axis,  $a$ , equal to the radius of the spherical region. Next, the shape tensor is recomputed using the elliptical norm,  $r_{e,n}^2 = x_n^2 + y_n^2/(b/a)^2 + z_n^2/(c/a)^2$ , instead of the radial distance  $r_n$ . The diagonalization procedure is repeated and new values of  $b/a$  and  $c/a$  are obtained. This procedure is iterated until the axes ratios converge to the desired accuracy. It should be noted that during this process, the mass inside the ellipsoid can indeed change, so strictly speaking, the value we use for the halo mass is not consistent with the ellipsoidal shape. However, the differences between these two quantities are at most 20% (see, e.g., Ref. [22]), which is much less than the variation across the halo population. Therefore, we do not implement any conversion between the halo mass inferred from the spherical BDM algorithm and the expected ellipsoidal counterpart.

### 3.3 Concentration parameter

The concentration values reported in the *Multidark Database* are computed for a spherical Navarro-Frenk-White (NFW) profile [81, 82],

$$\rho(r) = \frac{4\rho_s}{r/r_s(1+r/r_s)^2}, \quad (3.5)$$

where  $r$  is the distance to the center,  $\rho_s$  is the density at  $r_s$ , the scale radius, which corresponds to the distance at which the logarithmic slope of the profile is  $\frac{d \log \rho}{d \log r}(r_s) = -2$ .

Following the algorithm of Ref. [83], the halo concentration is defined from the ratio of the the maximum circular velocity,  $V_{\max}$ , to the circular velocity at the halo radius,  $V_v$ . For each halo the circular velocity  $V_{\text{circ}}(r) = \sqrt{GM(r)/r}$  is computed using the radial mass distribution  $M(r)$  for all bound particles. The separation of the radial bins is  $\Delta \log r/R_v = 0.01$ .

For the case of a spherical NFW density profile, the concentration is found by numerically solving the equation

$$\left(\frac{V_{\max}}{V_v}\right)^2 = \frac{0.2162 c_v}{f(c_v)}, \quad (3.6)$$

where  $f(c_v)$  is

$$f(c_v) = \ln(1 + c_v) - \frac{c_v}{1 + c_v}. \quad (3.7)$$

The results of this method are computationally robust, in contrast to more uncertain radial fitting methods that strongly dependent on the range used for the fit [47, 84]. The comparison of these two methods yield an offset  $< 15\%$ , where the concentrations derived with the velocities are higher. For halos with  $c_v < 5$  the offset is smaller than the intrinsic scatter at fixed halo mass [83].

On the other hand, in order to describe a triaxial halo we use a halo profile of the NFW form

$$\rho(r_e) = \frac{4 \rho_e}{c_e \frac{r_e}{r_v} \left(1 + c_e \frac{r_e}{r_v}\right)^2}, \quad (3.8)$$

where  $c_e$  is the concentration parameter in the triaxial case and the radial coordinate  $r$  is replaced by its ellipsoidal counterpart

$$r_e^2 = x^2 + \left(\frac{y}{b/a}\right)^2 + \left(\frac{z}{c/a}\right)^2, \quad (3.9)$$

where  $(x, y, z)$  are Cartesian coordinates. In order to be consistent with the halo mass inferred from the spherical BDM, the density at  $r_e = r_v/c_e$  ( $\rho_e$ ), is set by imposing the following condition on the halo mass:

$$M_v = \int dV \rho(r_e), \quad (3.10)$$

where  $dV$  is the spherical volume within a radius  $r_v$ .

The *Multidark Database* provides us with the halo mass  $M_v$ , the ratios of the axes,  $b/a$  and  $c/a$ , and concentration parameter  $c_v$ , obtained from Eq. (3.6) assuming a spherical NFW halo. However, in order to consistently define a triaxial halo, we need to determine the corresponding concentration parameter  $c_e$ . By numerically computing the ratio of  $V_{\max}$  and  $V_v$  for each halo with profile  $\rho(r_e)$  of Eq. (3.8) and equating it to the right-hand side of Eq. (3.6), we obtain  $c_e$ .

We have found numerically an approximate relation between  $c_e$  and  $c_v$ , which reads

$$c_e \simeq \left(\frac{b}{a} \frac{c}{a}\right)^{1/3} c_v. \quad (3.11)$$

The expression is accurate up to a precision of 3% - 15% in our sample. Heuristically, one can understand this relation by noting that the radius of a sphere with the same volume as the ellipsoid is  $r_{e,v} = [(b/a)(c/a)]^{1/3} r_v$ , so for the same scale radius,  $r_v/c_v = r_{e,v}/c_e$ , which is exactly Eq. (3.11).

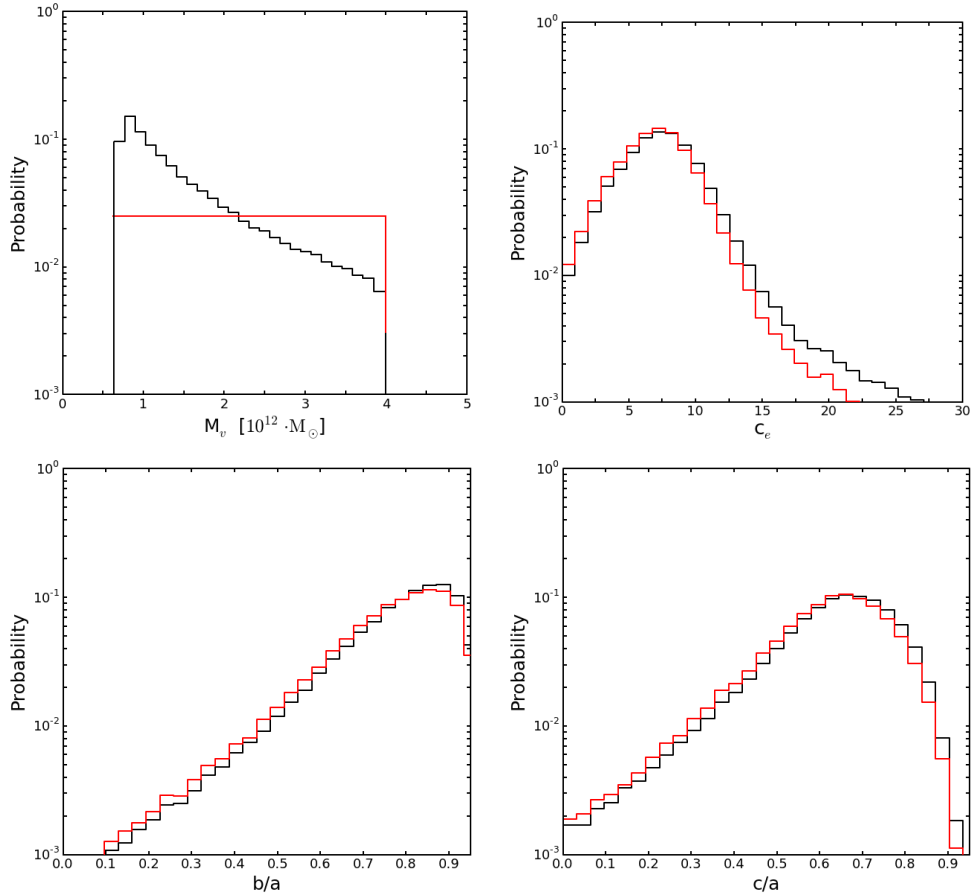


**Figure 1. Probability distributions of the halo parameters:** black lines for our final sample and red lines when a flat prior on  $M_v$  is imposed. The upper two panels depict the probability distributions of the halo mass  $M_v$  (left panel) and concentration parameter  $c_e$  (right panel). The lower two panels depict probability distributions of the axes ratios  $b/a$  (left panel) and  $c/a$  (right panel).

### 3.4 Data set

The original data set contains  $\sim 10^5$  halos which are selected to have masses in the Milky Way range, i.e.,  $M_v = [0.7, 4.0] \times 10^{12} M_\odot$ . However, the sample of halos has some spurious elements which cannot represent the Milky Way. For instance, as mentioned above, there are halos that are close to other massive structures and are truncated by the BDM algorithm. Therefore we discard halos with a radius  $r_v < 220$  kpc, which reduces the size of the original sample by  $\sim 5\%$ , thereby resulting in 87132 halos. The resulting distributions for the parameters of triaxial NFW profile are shown with the black lines in Fig. 1. The average values of the parameters in this sample are:  $\langle M_v \rangle = 1.55 \times 10^{12} M_\odot$ ,  $\langle c_e \rangle = 8.9$ ,  $\langle b/a \rangle = 0.81$  and  $\langle c/a \rangle = 0.66$ .

A useful way to characterize the shape of an ellipsoidal halo is by evaluating the so-called triaxiality parameter [85]

$$T = \frac{1 - (b/a)^2}{1 - (c/a)^2}. \quad (3.12)$$

An ellipsoid is considered prolate (sausage shaped) if  $a \gg b \approx c$  ( $1 > T > 2/3$ ), triaxial if



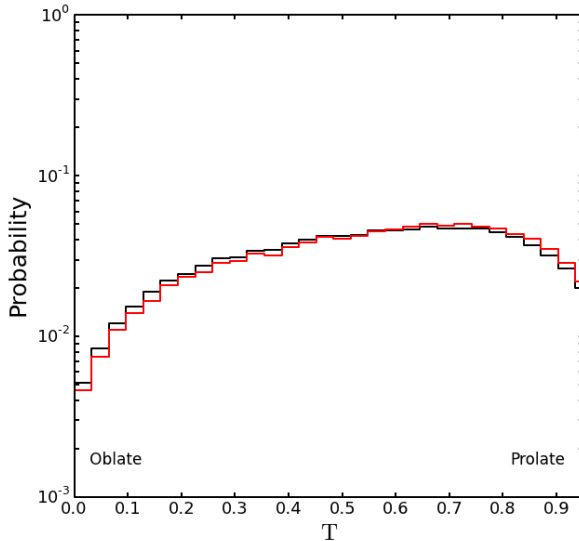


**Figure 2.** *Probability distribution of the triaxiality parameter ( $T$ )* in the data set. The black line represents our final sample and the red line represents the re-weighted sample with a flat prior on  $M_v$ .

$a > b > c$  ( $2/3 > T > 1/3$ ) and oblate (pancake shaped) if  $a \approx b \gg c$  ( $1/3 > T > 0$ ). It is well known that DM halos in N-body simulations which neglect possible baryonic effects, are in general triaxial: close to prolate in the central part and becoming rounder in the outer parts [7–25]. Numerical simulations with baryons produce shapes closer to spherical [26–30]. We show in Fig. 2 the distribution of the triaxial parameter  $T$  in our final sample, which has an average value of  $\langle T \rangle = 0.58$ .

Hierarchical structure formation predicts that massive halos are formed by mergers of smaller halos. This feature is nicely illustrated in the probability distribution of  $M_v$  in Fig. 1. A larger number of halos exist for low masses. This dependence of the halo abundance as a function of halo mass is well understood and is parametrized through the halo mass function. However, as for the Milky Way, its mass is quite uncertain (within an order of magnitude). In order to avoid an unfair weight to the low mass range due to cosmological effects in the simulation, we also consider a flat prior on  $M_v$  by weighting all bins such that all values of  $M_v$ , in the range  $M_v = [0.7, 4.0] \times 10^{12} M_\odot$ , are equiprobable. With such an exercise we can study systematic effects independently of the cosmological bias. The probability distributions of the parameters for this re-weighted sample, with a flat prior on the halo mass, are depicted in Figs. 1 and 2 with the red curves.

#### 4 Impact of halo asphericity

In this section we describe the possible impact of having a non-spherical halo on quantities such as the local DM density ( $\rho_\odot$ ) and  $J$  factors. Consider a set of observers at a given distance from the halo center who are able to locally measure properties of the halo and are able to compute  $\rho_\odot$ . In a spherically symmetric halo all observers would obtain the same value. However, in a triaxial halo these measurements would lead to a significant variance with respect to the spherically averaged value [86]. We show that there exists similar deviations from the spherically averaged value for  $J$  factors as well.

Halo Type	$M_v$ [ $10^{12} M_\odot$ ]	$R_v$ [kpc]	$c_e$	$b/a$	$c/a$
Approx. Spherical	3.8	242	9.73	0.97	0.91
Prolate	3.6	404	5.33	0.58	0.48
Oblate	2.0	419	9.79	0.97	0.77

**Table 1.** Parameters of the example halos used to illustrate the impact of asphericity in Fig. 3.

In order to illustrate this, we consider three example halos: an almost spherical halo, a prolate halo and an oblate halo; which are described by the parameters in Table 1. A typical ellipsoid is defined by three axes of symmetry, the major axis ( $a$ ), intermediate axis ( $b$ ) and the minor axis ( $c$ ). Correspondingly there exists three orthogonal planes denoted by  $a - b$ ,  $a - c$  and  $b - c$ . We assume the galactic disc to coincide with one of the symmetry planes of the dark halo, although this is not guaranteed [43, 87]. However, due to the lack of a definite solution to the problem of the shape and orientation of the halo, we assume the alignment of the stellar disc with one of the three symmetry planes of the halo in order to bracket the uncertainties. Consequently, our ignorance of where the solar system might reside in a triaxial halo motivates us to evaluate the aforementioned quantities individually for each plane of symmetry.

With the halo profile exactly defined by  $M_v$ ,  $c_e$ ,  $b/a$  and  $c/a$ , we proceed to compute the local DM density,  $\rho_\odot$ , and the  $J$  factors for a region of interest (ROI) of  $3^\circ \times 3^\circ$  (a square of  $3^\circ$  side) around the galactic center. We do so for different points along a circle of radius  $R_\odot$  ( $= 8.3$  kpc) for the three planes of symmetry. Then, we compute the average quantities in a spherical shell of the same radius<sup>2</sup>,  $\langle \rho_\odot \rangle$ ,  $\langle \bar{J}_{\text{ann}} \rangle$  and  $\langle \bar{J}_{\text{dec}} \rangle$ . The results corresponding to the three halos (one approximate spherical, one prolate and one oblate) defined in Table 1 are depicted in Fig. 3, where we show the deviation of each quantity with respect to its spherical average as a function of the angular position  $\theta$  along a circle of radius  $R_\odot$ . We choose  $\theta = 0$  as a reference point, which corresponds to the occurrence of the maximum value of each quantity. In all panels, the solid red, dashed blue and dotted black curves indicate the variation along the  $a - b$  plane, the  $a - c$  plane and the  $b - c$  plane, respectively.

As expected, the deviations from the spherical average are the smallest for the approximately spherical halo (left panels in Fig. 3). A maximum variation of  $\sim 5\%$  for the local DM density is found and only  $\sim 1.6\%$  and  $\sim 2.5\%$  for  $\bar{J}_{\text{ann}}$  and  $\bar{J}_{\text{dec}}$ , respectively. On the other hand, in the case of the prolate halo we consider here (middle panels in Fig. 3), deviations of up to  $\sim 46\%$ ,  $\sim 14\%$  and  $\sim 20\%$  are possible for  $\rho_\odot$ ,  $\bar{J}_{\text{ann}}$  and  $\bar{J}_{\text{dec}}$ , respectively. The oblate halo (right panels in Fig. 3), being closer to the spherical case, presents deviations of up to  $\sim 20\%$ ,  $\sim 6\%$  and  $\sim 9\%$  for  $\rho_\odot$ ,  $\bar{J}_{\text{ann}}$  and  $\bar{J}_{\text{dec}}$ , respectively.

A common feature among the different quantities shown in Fig. 3 is their angular dependence, i.e., the peaks and troughs occur at the same angular position. This is related to the exact position of observation on a given plane. As we move around a circle of radius  $R_\odot$  from the galactic center, the angular dependence is periodic. The amplitude is proportional

<sup>2</sup>The average density  $\langle \rho_\odot \rangle$  is the quantity inferred from dynamical measurements in the galaxy.

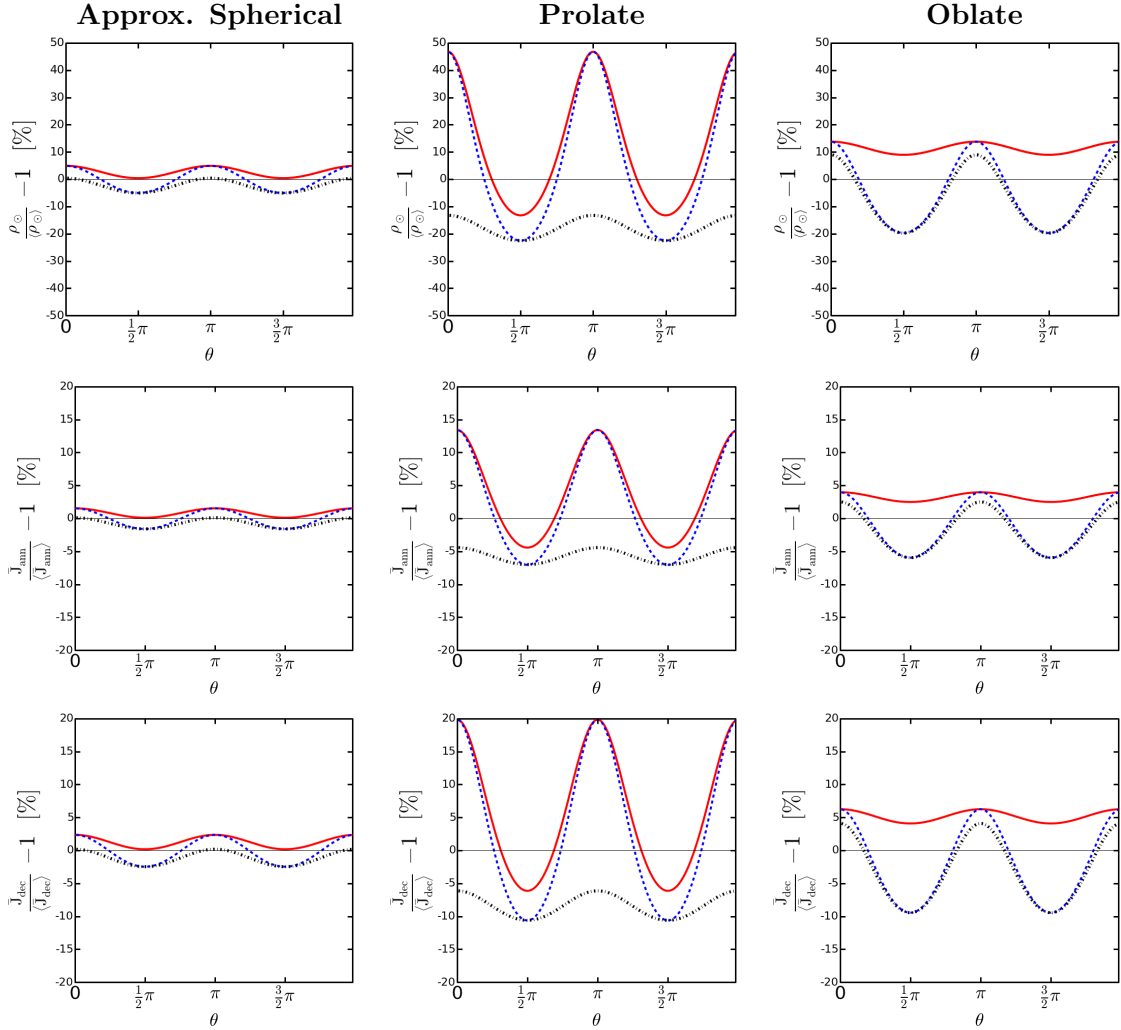


**Figure 3.** *Deviation from the average in a spherical shell of radius  $R_\odot$  for the three symmetry axes.* We show the results for three quantities:  $\rho_\odot$  (top panels),  $\bar{J}_{\text{ann}}$  (middle panels) and  $\bar{J}_{\text{dec}}$  (bottom panels) for a square ROI of  $3^\circ \times 3^\circ$  around the galactic center. Each column refers to a given halo: approximately spherical halo (left column), prolate halo (middle column) and oblate halo (right column). In all panels, the  $a-b$  plane is represented by the solid red curve, the  $a-c$  plane by the dashed blue curve and the  $b-c$  plane by the dotted black curve. The angle  $\theta$  represents the angular position along a circle of radius  $R_\odot$  for each plane of symmetry.

to the overall normalization, which in turn depends on the shape of the halo. For example, oblate halos have larger deviations from the spherical average on the  $b-c$  plane than on the  $a-b$  plane. This trend is inverted for a prolate halo. Let us also note that the deviations for the  $J$  factors are larger for DM decay than for DM annihilation. Heuristically, this can be understood by considering the contributions to the  $J$  factors away from the center of the halo. As the flux from DM annihilations depends on the square of the DM density distribution, in contrast to the linear dependence for DM decays. For DM annihilations, the relative contribution to the  $J$  factors from the outer regions (i.e., regions which are closer to the boundary of the ROI) with respect to the contribution from the center is expected to be

smaller than for DM decays. Hence, the deviations from the spherical average are smaller for DM annihilations. This is seen in Fig. 3 and below when discussing our results.

The point emphasized by this exercise is that halo asphericity could give rise to significant deviations from the spherically averaged values of relevant quantities for DM searches. Indeed, these deviations could be quite large depending on the shape of the halo and could have a substantial impact on direct and indirect DM detection. In the following, we quantify these uncertainties statistically by using the whole halo data set.

## 5 Observational priors

In addition to showing results for the original sample from the *MultiDark Database*, which represents a selection of halos in a mass range compatible with the mass of the Milky Way, we also consider several observational constraints and show results after applying the corresponding priors. In addition to a prior on the virial mass, we also include priors on the enclosed mass at 60 kpc, the local DM surface density and the Sun’s galactocentric distance. We add flat priors for the virial mass (to compensate for the cosmological bias) and the Sun’s distance to the galactic center. Gaussian priors are used for the other two observables. Hence, for each plane of symmetry, the probability distribution function of the original data sample is modified as:

$$\begin{aligned} \text{PDF}_{\text{prior}}^p(\vec{\omega}) &= C \frac{\text{PDF}(\vec{\omega})}{\text{PDF}(M_v)} \times \theta(M_v - M_v^{\min}) \theta(M_v^{\max} - M_v) \\ &\times \int_{R_{\odot}^{\min}}^{R_{\odot}^{\max}} dR_{\odot} \exp \left[ -\frac{(M_{60}^{\text{DM}} - M_{60})^2}{2\sigma_{60}^2} \right] \\ &\times \int_0^{2\pi} d\psi \exp \left[ -\frac{(\Sigma_{1.1}^{\text{DM}} - \Sigma_{1.1}^p(R_{\odot}, \psi))^2}{2\sigma_{\Sigma}^2} \right], \end{aligned} \quad (5.1)$$

where  $C$  is a normalizing constant,  $\vec{\omega} = (M_v, c_e, b/a, c/a)$ ,  $\text{PDF}(\vec{\omega})$  is the original probability distribution function and  $\text{PDF}(M_v)$  is the probability distribution function after marginalizing over  $(c_e, b/a, c/a)$ .  $\text{PDF}_{\text{prior}}^p(\vec{\omega})$  is computed for the three symmetry planes,  $p = a - b$ ,  $a - c$  and  $b - c$ , where  $\psi$  is the azimuthal angle at the solar circle. The limits, central values and errors, discussed below, are indicated in Tab. 2. Note that the prior on  $M_{60}$  is a global prior for a given halo, whereas the prior on the DM surface density is a local constraint which depends on the exact position of the observer in the halo and thus, on the plane of symmetry under consideration. Given a triaxial halo, the value of the surface density at various angular points can be significantly different.

### 5.1 The virial mass of the Milky Way

We have selected our data set by the criterion of halo mass (see Sec. 3). Observationally, different methods have been used to determine the mass of the Milky Way, such as gravitational lensing, gas rotation curves, escape velocity arguments or Jeans modeling of the radial density and velocity dispersion profiles of kinematic tracers (blue horizontal branch stars, carbon stars, asymptotic giant branch stars, globular clusters, satellite galaxies), or timing arguments. In general, estimates based on stellar kinematics tend to yield a low mass,  $\lesssim 10^{12} M_{\odot}$  [88–92], but usually infer the total mass from an extrapolation from the inner halo to the virial radius using models for the different components of the Milky Way. However, estimates based on distant tracers, such as globular clusters or satellite galaxies, and on statistics

	Gaussian priors		Flat priors	
	Central value	$1\sigma$ error	Lower cut	Upper cut
Virial mass [ $10^{12} M_{\odot}$ ]	–	–	$M_v^{\min} = 0.7$	$M_v^{\max} = 4.0$
DM mass within 60 kpc [ $10^{11} M_{\odot}$ ]	$M_{60}^{\text{DM}} = 4.0$	$\sigma_{60} = 0.7$	–	–
Local DM surface density [ $M_{\odot} \text{pc}^{-2}$ ]	$\Sigma_{1,1}^{\text{DM}} = 17$	$\sigma_{\Sigma} = 6$	–	–
Sun’s galactocentric distance [kpc]	–	–	$R_{\odot}^{\min} = 7.5$	$R_{\odot}^{\max} = 9$

**Table 2.** Limits for the halo virial mass ( $M_v$ ) and the Sun’s galactocentric distance ( $R_{\odot}$ ) and central values and  $1\sigma$  errors for the DM halo mass at 60 kpc ( $M_{60}^{\text{DM}}$ ) and the local DM surface density ( $\Sigma_{1,1}^{\text{DM}}$ ), which are used for the priors discussed in the text.

of cosmological DM simulations tend to imply larger masses,  $\gtrsim 10^{12} M_{\odot}$  [93–100], but there are few distant tracers beyond  $\sim 80$  kpc, where the DM dominates. There are, though, exceptions in both cases [101–106] and combinations of these data sets to obtain rotation curves up to large distances allow for a wide range of values based on modeling [107–113]. Fitting of dynamical models with kinematic and photometric data tends to provide best fit values above  $10^{12} M_{\odot}$  [2–6]. On the other hand, more indirect determinations can be obtained from combinations of galaxy-galaxy lensing and Tully-Fisher data [114, 115] or from the relation of the halo mass and the stellar mass [116–118], both predicting a mass of the Milky Way above  $10^{12} M_{\odot}$ . From all these results, the virial mass of the Milky Way is expected to lie within a large range of values,  $8 \times 10^{11} < M_v/M_{\odot} < 3 \times 10^{12}$ . In this work we have selected a data set from the *MultiDark Database*, which covers the mass interval  $M_v = [0.7, 4.0] \times 10^{12} M_{\odot}$  and, as discussed in Sec. 3, we use a flat prior for this interval in order to compensate the cosmological bias which favors low mass halos.

## 5.2 The mass of the Milky Way within 60 kpc

Within the innermost  $\sim 80$  kpc of the Milky Way there are numerous kinematic tracers, beyond this distance there are only a few known globular clusters and satellite galaxies (see Ref. [90], for instance). This introduces significant errors when estimating the total mass of the Milky Way. Therefore, we expect the estimate of the mass in the inner  $\sim 50 - 80$  kpc to suffer from fewer uncertainties. This mass has been determined using kinematic data of halo stars [89, 90, 92–94, 102, 104]. In this work we consider the result based on a set of 2401 blue horizontal-branch halo stars from the Sloan Digital Sky Survey with distances from the galactic center up to  $\sim 60$  kpc [89],  $M_{60} \equiv M(< 60 \text{ kpc}) = (4.0 \pm 0.7) \times 10^{11} M_{\odot}$ , and implement Gaussian priors. Let us note that  $M_{60}$  is the total mass within 60 kpc and that the galactic disc and bulge (visible matter) are estimated to contribute with a total mass of about an order of magnitude lower,  $\sim (5 - 7) \times 10^{10} M_{\odot}$  [5, 62, 119, 120], which represents approximately the  $1\sigma$  error on  $M_{60}$ . We do not correct for this difference, i.e., we take  $M_{60}^{\text{DM}} = M_{60}$ .

### 5.3 Local DM surface density

The mass distribution of the Milky Way in the local neighborhood can be characterized by the local surface density to some distance  $|z| = z_0$ ,

$$\Sigma_{z_0}(\mathbf{R}_\odot) \equiv \Sigma(\mathbf{R}_\odot, |z| < z_0) = \int_{-z_0}^{+z_0} \rho(\mathbf{R}_\odot, z) dz, \quad (5.2)$$

where the integration limit is conventionally taken to be  $z_0 = 1.1$  kpc.

From the determination of the vertical gravitational potential using stellar dynamics, the total local surface density to  $|z| = 1.1$  kpc has been inferred to lie within  $\Sigma_{1.1}(\mathbf{R}_\odot) \simeq 60 - 80 M_\odot \text{pc}^{-2}$  [59, 61, 62, 121–124]. However, establishing which fraction belongs to the dark halo or to the baryonic disc (stars and gas) requires further modeling. The local disc surface density is found to be  $\Sigma_{1.1}^d(\mathbf{R}_\odot) \simeq 45 - 55 M_\odot \text{pc}^{-2}$  [51, 52, 59, 61–64, 121, 125, 126]. Unlike dynamical determinations of the total disc surface density, direct observations of local stars are expected to induce smaller uncertainties on the contribution from the visible stellar matter,  $\Sigma_{1.1}^{\text{visible}} \sim 25 - 30 M_\odot \text{pc}^{-2}$  [58, 120, 127–130]. An additional contribution of  $\sim 5 - 7 M_\odot \text{pc}^{-2}$  is estimated to come from stellar remnants and brown dwarfs [59, 120], and  $\sim 13 - 15 M_\odot \text{pc}^{-2}$  [58, 131] from the interstellar gas.

We use the recent results of Ref. [62], obtained after dynamical modeling and based on a large data set of phase-space of individual stars. The total local surface density is determined to be  $\Sigma_{1.1}(\mathbf{R}_\odot) = (68 \pm 4) M_\odot \text{pc}^{-2}$ , of which  $(38 \pm 4) M_\odot \text{pc}^{-2}$  is contributed by stars and stellar remnants. A contribution of  $13 M_\odot \text{pc}^{-2}$  from the thin gas layer is assumed. Thus implying a DM halo contribution  $\Sigma_{1.1}^{\text{DM}}(\mathbf{R}_\odot) = (17 \pm 6) M_\odot \text{pc}^{-2}$ .

### 5.4 Sun’s galactocentric distance

Based on an old recommendation of the International Astronomical Union, the Sun’s galactocentric distance is usually assumed to be  $R_\odot = 8.5$  kpc [132]. This number was obtained as a result of an average of different estimates after 1974. However, a more careful analysis of estimates between 1974 and 1993 rendered a lower value,  $R_\odot = 8.0 \pm 0.5$  kpc [133] and with new measurements, about a decade ago, the average value was  $R_\odot = 7.9 \pm 0.2$  kpc [134] (see also Ref. [135]).

In recent years, many new measurements have been published. Different methods exist to determine  $R_\odot$  (see Ref. [136] for a compilation of  $R_\odot$  measurements since 1918). One of them is the halo centroid method, based on the mean distance of globular clusters [136, 137], which tends to give low values,  $R_\odot \sim 7.2 - 7.4$  kpc. Another method uses the luminosity distance of bulge stars, such as RR Lyrae, Cepheids, Delta Scuti, the red clump, Mira stars or planetary nebula. The measured value varies over a relatively large range,  $R_\odot \sim 7.4 - 8.8$  kpc [136, 138–150], probably caused by systematics associated to the calibration of magnitudes [136]. The solar-circle (or its modification, the near-solar circle) method is a geometrical method which requires no other assumption but circular motion [151–153] and obtains a Sun’s galactocentric distance in the range  $R_\odot \sim 7.3 - 7.8$  kpc. Other pure geometrical approaches obtain  $R_\odot \sim 8.3$  kpc [154, 155]. In addition to these indirect methods, there are others based on the direct determination of this distance. Measurements with trigonometric parallax of water masers near the center of the galaxy might be the ideal method, although with its current precision it is not competitive [156]. Another method is based on spectroscopic information of parallax and proper motions of regions of high-mass star formation, along with modeling of the rotation curve [157–160]. Recently, there has been some controversy regarding the value of the solar

motion component in the direction of the galactic rotation [161], which is correlated with  $R_\odot$ , and on the sensitivity to the parametrization of the rotation curve. This has been discussed in detail in a new analysis that has obtained  $R_\odot = 8.34 \pm 0.16$  [162]. Finally, astrometric and radial velocity measurements of the Milky Way nuclear star cluster, around the black hole in the galactic center, measure a similar distance,  $R_\odot \sim 8.3 - 8.5$  kpc [163–166], although this measurement is strongly correlated with the mass of the central black hole. All in all, estimates based on direct distance measurements seem to converge to  $R_\odot \sim 8.3$  kpc, whereas more indirect methods tend to obtain values in the range  $R_\odot \sim 7.5 - 8.2$  kpc. In this work, we consider the range  $R_\odot = [7.5, 9.0]$  kpc, and use a flat prior.

## 6 Results

Using the complete set of parameters, which define the ellipsoidal NFW profile for each halo in the simulation sample, we evaluate the probability distribution of variations with respect to the spherically averaged quantities of interest in this work: the local DM density and the so-called  $J$  factors in indirect DM searches. We show results for the case when no priors are considered, i.e., just the bare distributions from the simulation sample are used to quantify the systematic effects. And we also show results for the case when we make use of observational information and analyze the data by adding priors on different quantities, which weigh the original probability distributions, as described above.

### 6.1 Systematic uncertainties on $\rho_\odot$

As already mentioned, the value of  $\rho_\odot$  deduced from most dynamic measurements often refers to the spherically averaged density  $\langle \rho_\odot \rangle$ . We also noted that, in a non-spherical halo, the actual DM density in the solar neighborhood could actually differ significantly from that value (see Sec. 4). Here, we consider the whole sample of halos from the *MultiDark Database* and study this type of uncertainties as a function of the local average of the DM density.

The spherically averaged local DM densities,  $\langle \rho_\odot \rangle$ , at distance  $R_\odot$  are computed for all halos in our data set, using the parameters that fit each halo with the triaxial density profile given by Eq. (3.8). All halos are binned according to their value of the spherical average  $\langle \rho_\odot \rangle$ . Then, for every halo,  $\rho_\odot$  is evaluated in a grid of 300 different points along a circle of radius  $R_\odot$  for each plane of symmetry and for 6 values of  $R_\odot$  covering the range in Tab. 2. The results for the deviations from the spherically averaged value are depicted in Fig. 4. The left and right columns correspond to cases without and with priors, respectively. In this figure, we show the deviation of  $\rho_\odot$  from its spherically averaged value  $\langle \rho_\odot \rangle$  for the three symmetry planes as a function of  $\langle \rho_\odot \rangle$ . The dark blue (light orange) contours represent the 68% (95%) most probable regions of the deviation. On the top and the right of each panel the projected probability distributions of  $\langle \rho_\odot \rangle$  and  $\frac{\rho_\odot}{\langle \rho_\odot \rangle} - 1$  are depicted, respectively.

In the principal plane  $a - b$ , the local density tends to adopt values larger than those of the average density, whereas in the plane  $b - c$  the values are typically smaller than the average. The deviations (in absolute value) in the  $a - b$  plane are larger compared to the ones in the  $b - c$  plane due to the fact that there are more prolate than oblate halos (see Figs. 2 and 3). The densities in the plane  $a - c$  are intermediate, spanning over a large range that goes from the lowest values reached in the  $b - c$  plane to the highest values in the  $a - b$  plane.

Fig. 4 shows important deviations with respect to the spherically averaged local DM density, especially for low values,  $\langle \rho_\odot \rangle \lesssim 0.2$  GeV/cm<sup>3</sup>. Such small values for  $\langle \rho_\odot \rangle$  are common in very triaxial halos which, in turn, naturally generate large deviations. We also note that



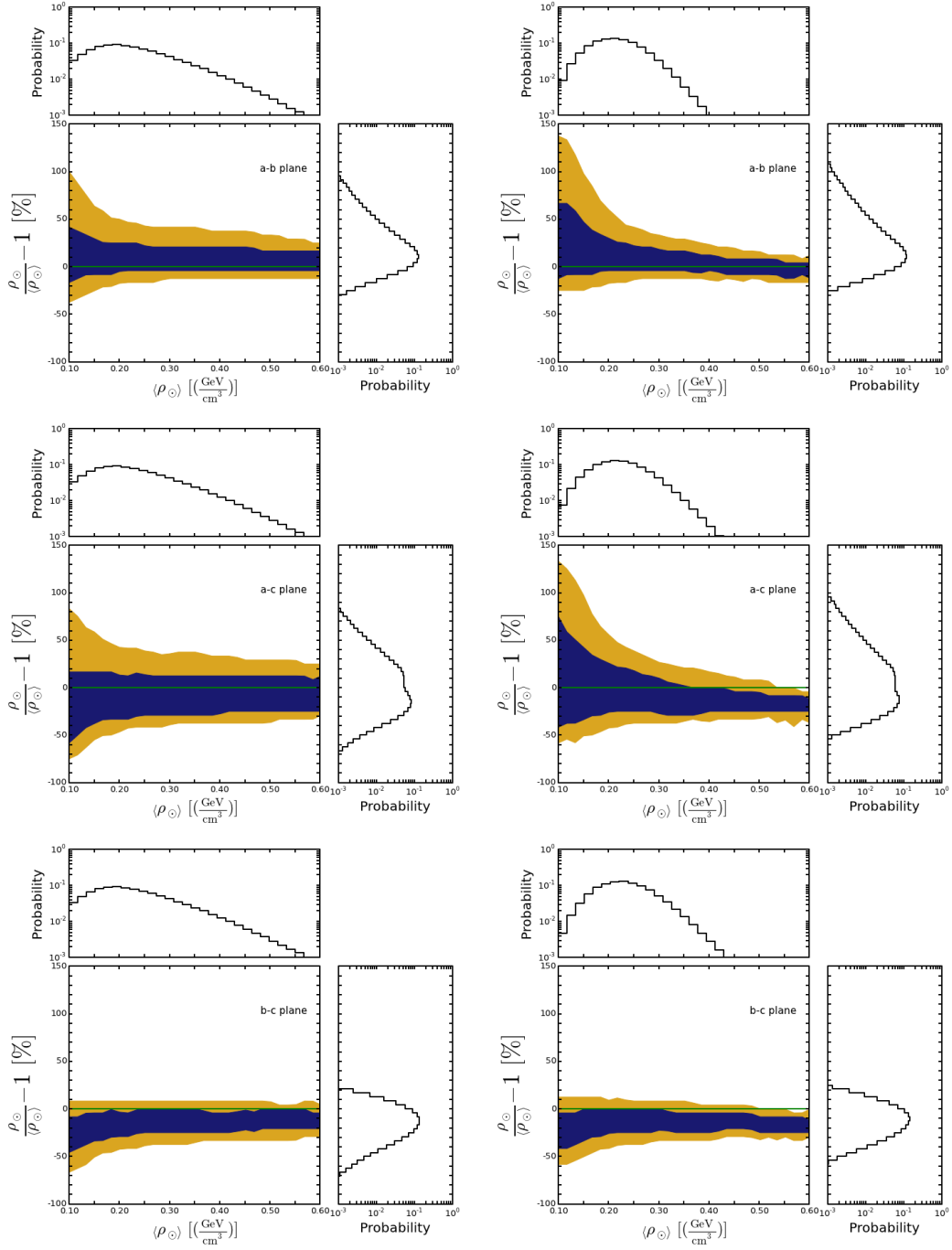


**Figure 4.** *Systematic uncertainties on  $\rho_{\odot}$ , stemming from the non-sphericity of the Milky Way DM halo.* We show the probability distribution of the deviation of the local DM density from its spherically average value,  $\langle\rho_{\odot}\rangle$ , for the three symmetry planes as a function of  $\langle\rho_{\odot}\rangle$ . The left (right) panels depict the results for the case without (with) priors included. The dark blue (light orange) contours represent the 68% (95%) most probable regions. On the top and the right of each panel we depict the projected probability distribution with respect to that quantity.



for the case without priors, for values of the average local DM density above  $\sim 0.2 \text{ GeV/cm}^3$  the deviations do not change significantly, being of the order of  $\begin{matrix} +20\% & (+40\%) \\ -5\% & (-15\%) \end{matrix}$ ,  $\begin{matrix} +15\% & (+35\%) \\ -30\% & (-40\%) \end{matrix}$  and  $\begin{matrix} +0\% & (+10\%) \\ -30\% & (-35\%) \end{matrix}$  for the 68% (95%) most probable regions in the  $a - b$  plane,  $a - c$  plane and  $b - c$  plane, respectively.

A few differences are observed when priors are added. The prior on  $M_{60}$  mostly affects the probability distribution of  $\langle \rho_{\odot} \rangle$ , which gets narrower and tends to peak around  $\sim 0.20 - 0.25 \text{ GeV/cm}^3$ . Let us recall that the prior on  $M_{60}$  is independent of the point of observation and only depends on the global properties of the halo. However, the prior on the value of the surface density,  $\Sigma_{1,1}^{\text{DM}}$ , has a strong influence on the distribution of  $\rho_{\odot}/\langle \rho_{\odot} \rangle - 1$ . The uncertainties on  $\rho_{\odot}$  tend to be slightly smaller for intermediate and high values of  $\langle \rho_{\odot} \rangle$  and slightly larger for low values of  $\langle \rho_{\odot} \rangle$ , although the differences, in general, are not very significant.

## 6.2 Systematic uncertainties on $\bar{J}_{\text{ann}}$ and $\bar{J}_{\text{dec}}$

Analogously to the analysis performed to estimate the uncertainties on the local DM density (Fig. 4), we also compute the systematic uncertainties, caused by the non-sphericity of the Milky Way DM halo, on the determination of the  $J$  factors for DM annihilation and decay. Our results are depicted in Fig. 5 for  $\bar{J}_{\text{ann}}$  and in Fig. 6 for  $\bar{J}_{\text{dec}}$ , as a function of their spherically averages,  $\langle \bar{J}_{\text{ann}} \rangle$  and  $\langle \bar{J}_{\text{dec}} \rangle$ , for the three symmetry planes and for a square ROI of  $3^\circ \times 3^\circ$  around the galactic center. The left (right) panels correspond to the case without (with) priors. The blue (orange) regions represent the 68% (95%) most probable contours. These figures have essentially the same features of Fig. 4: for intermediate and high values of  $\langle \bar{J} \rangle$ , approximately the same uncertainty is found, whereas larger errors are obtained for low values<sup>3</sup> of  $\langle \bar{J} \rangle$ . For DM annihilations (Fig. 5) and for intermediate and high values of  $\langle \bar{J}_{\text{ann}} \rangle$ , the deviations are of the order of a few percent (up to  $\sim 10\%$ ) for the 68% (95%) most probable regions. On the other hand, for DM decays (Fig. 6), the deviations from the average value for intermediate and high  $\langle \bar{J}_{\text{dec}} \rangle$ , are of the order of a few percent, up to  $\sim 10\%$  (up to  $\sim 15\%$ ) for the 68% (95%) most probable regions. The inclusion of priors has a very similar effect to what happens for the local DM density. The prior on  $M_{60}^{\text{DM}}$  gives more weight to low values of the  $J$  factors and makes the probability distribution narrower, whereas the prior on  $\Sigma_{1,1}^{\text{DM}}$  makes the variations of the  $J$  factors to be slightly smaller for intermediate and high values and larger for low values. All in all, the inclusion of priors produces small changes with respect to the results without priors. Finally, let us stress that we have verified that the variations with respect to the average value for the  $J$  factors depend very weakly on the chosen ROI (around the galactic center).

In order to serve as a reference, let us note that the  $J$  factors for the same ROI, corresponding to a spherical NFW profile with  $r_s = 20 \text{ kpc}$  and  $\rho_{\odot} = 0.3 \text{ GeV/cm}^3$  at  $R_{\odot} = 8.3 \text{ kpc}$ , are:  $\langle \bar{J}_{\text{ann}} \rangle = 590 (\text{GeV/cm}^3)^2 \text{ kpc}$  and  $\langle \bar{J}_{\text{dec}} \rangle = 43 (\text{GeV/cm}^3) \text{ kpc}$ .

<sup>3</sup>The bump in Fig. 6, which occurs at very low values of  $\langle \bar{J}_{\text{dec}} \rangle$ , is due to the presence of a small number of approximately spherical halos with very large concentrations in the first bin, which further get favorably weighted by the priors. It is a statistical effect due to the finite size of the sample and the chosen size of the bins. It does not show up in Fig. 5 because the number of halos in the first bin is two orders of magnitude larger.

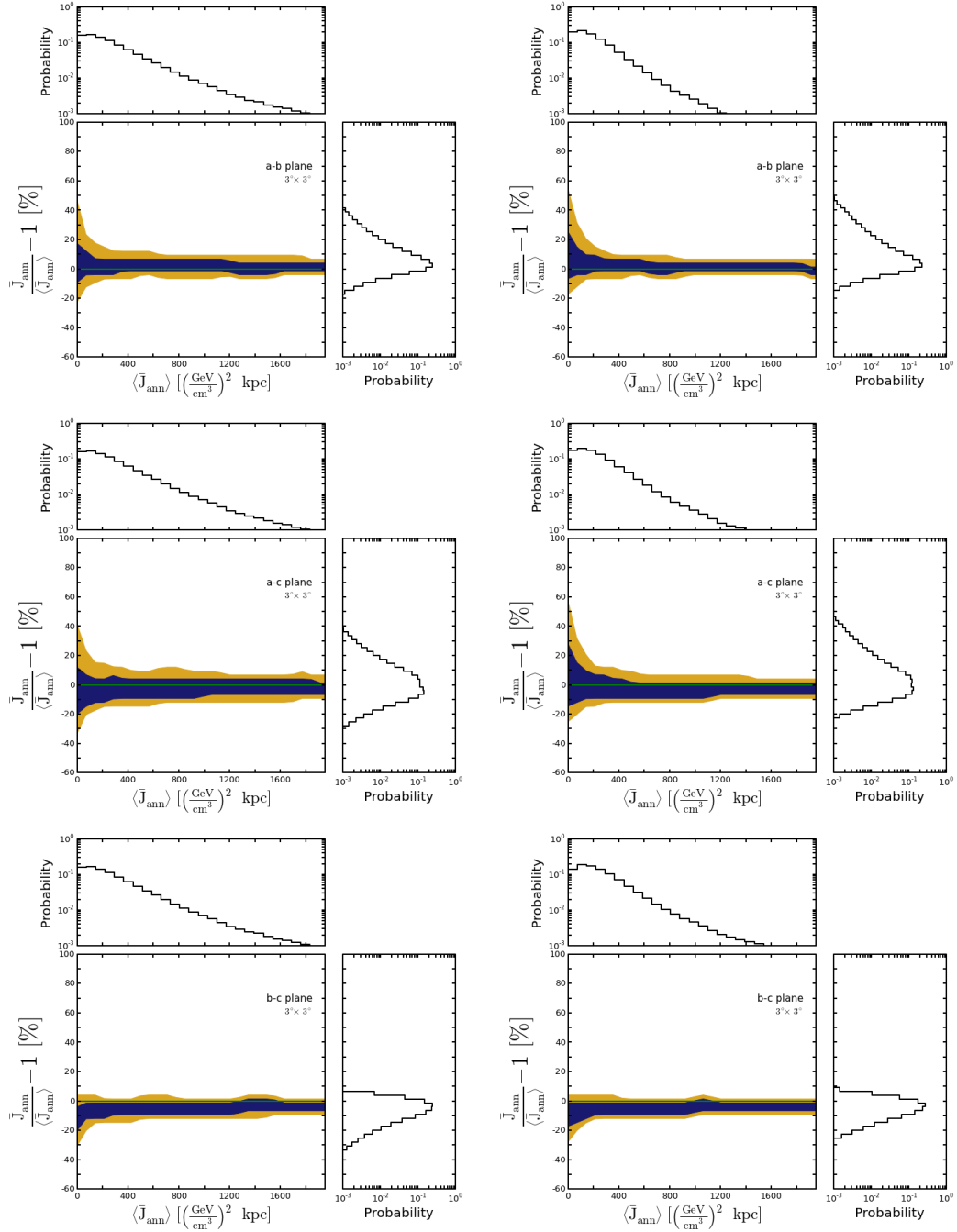
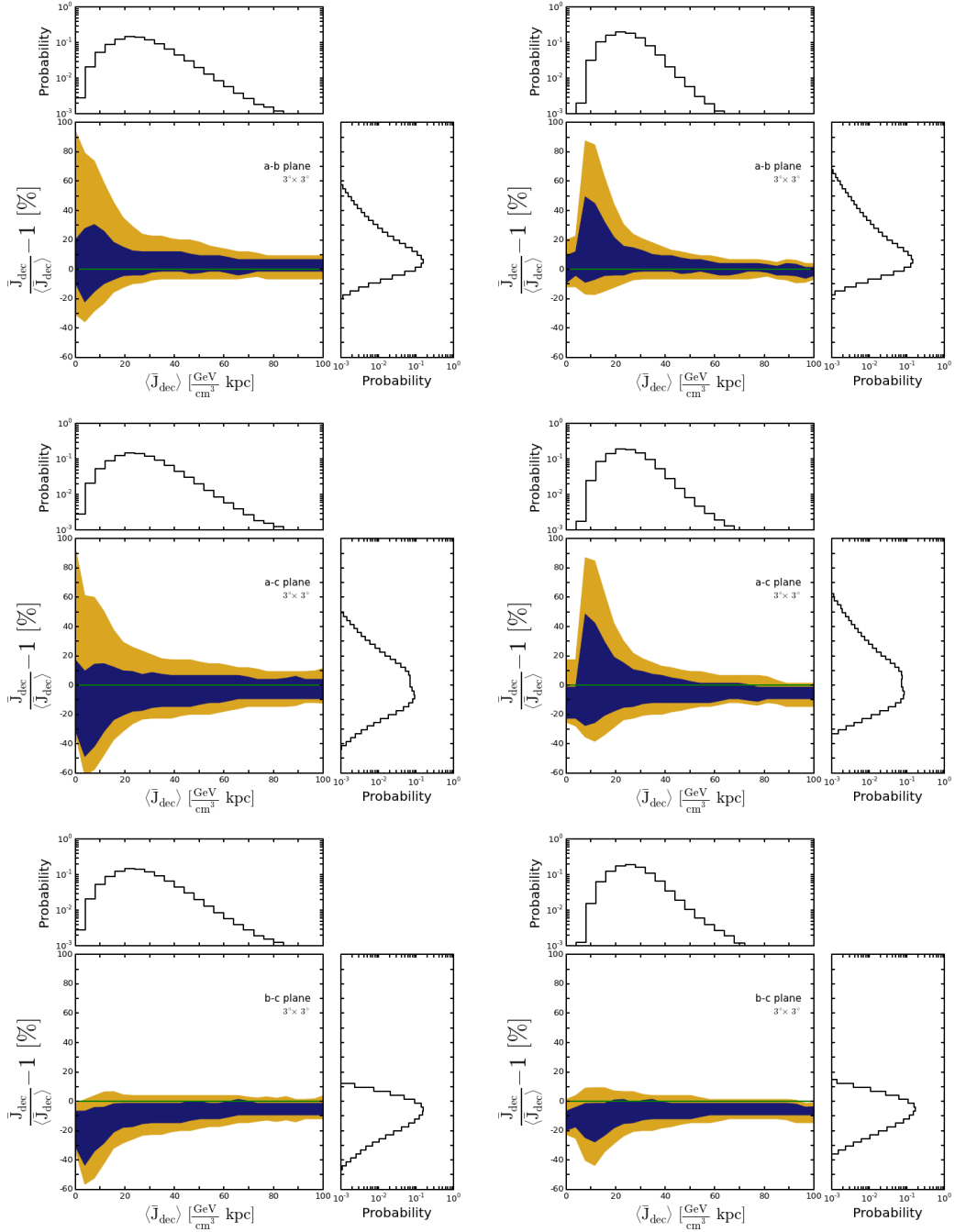


Figure 5. *Systematic uncertainties on  $\bar{J}_{\text{ann}}$  for a square ROI of  $3^\circ \times 3^\circ$  around the galactic center for DM annihilations, stemming from the non-sphericity of the Milky Way DM halo.* We show the probability distribution of the deviation of  $\bar{J}_{\text{ann}}$  from its spherically average value,  $\langle \bar{J}_{\text{ann}} \rangle$ , for the three symmetry planes as a function of  $\langle \bar{J}_{\text{ann}} \rangle$ . The panels and colors of the different contours represent the same as in Fig. 4.



**Figure 6.** *Systematic uncertainties on  $\bar{J}_{\text{dec}}$  for a square ROI of  $3^\circ \times 3^\circ$  around the galactic center for DM decays, stemming from the non-sphericity of the Milky Way DM halo.* We show the probability distribution of the deviation of  $\bar{J}_{\text{dec}}$  from its spherically average value,  $\langle \bar{J}_{\text{dec}} \rangle$ , for the three symmetry planes as a function of  $\langle \bar{J}_{\text{dec}} \rangle$ . The panels and colors of the different contours represent the same as in Fig. 4.

## 7 Discussion and Conclusions

Direct and some indirect strategies of DM searches depend on its spatial distribution in the galaxy. If a DM signal is detected, one of the main focus of these searches would be to deduce properties of the DM particle. Otherwise, the non-observation of a signal could be used to derive upper limits on the DM annihilation and scattering cross section. In the case of DM direct detection, the event rate is directly proportional to the local DM density,  $\rho_{\odot}$ , as described in Sec. 2. Therefore, any systematic error on  $\rho_{\odot}$  translates into an error on the limits (or measurement) of the scattering cross section. Similarly, for indirect detection, the gamma-ray and neutrino flux from DM annihilations or decays is directly proportional to the so-called  $J$  factors. The error on them directly translates into an error on the limits (or measurement) of the thermally averaged DM annihilation cross section and on the DM mean lifetime.

Although DM halo profiles are usually assumed to be spherical, it is well known that N-body simulations predict halos to be non-spherical [7–25]. In this work we consider a very large sample of  $\sim 10^5$  DM-only halos (described in Sec. 3), from the N-body cosmological simulation *Bolshoi* [47], publicly available through the *MultiDark Database*, with masses in the range of that of the Milky Way. We construct the probability distributions of the parameters that define their shape and use them to study the impact of halo asphericity on the determination of the local DM density and the  $J$  factors relevant for indirect searches of signals from the galactic center. This is first illustrated in Sec. 4 with three example halos: an approximately spherical halo, a prolate halo and an oblate halo.

In addition to the halo sample obtained from the N-body simulation, we also add several observational constraints: on the virial mass, on the enclosed mass at 60 kpc, on the local DM surface density and on the Sun’s galactocentric distance. All these constraints and the way we implement them are described in Sec. 5.

Finally, in Sec. 6 we show our results without and with observational priors included, although the differences are small. We have shown that, including priors, for values of the spherical average of the local DM density of the order of current estimates, i.e.,  $\langle\rho_{\odot}\rangle \simeq 0.3 - 0.4 \text{ GeV/cm}^3$ , the actual value of  $\rho_{\odot}$ , if the stellar disk coincides with the  $a - b$  plane of the DM halo, with a probability of 95%, lies in the interval (see upper right panel of Fig. 4)

$$\frac{\rho_{\odot}}{\langle\rho_{\odot}\rangle} = 0.83 - 1.35 , \quad (7.1)$$

in rough agreement with Refs. [44, 45]. On the other hand, if the stellar disk coincides with the  $a - c$  ( $b - c$ ) plane the range, with a probability of 95%, the range is  $\rho_{\odot}/\langle\rho_{\odot}\rangle = 0.62 - 1.27$  ( $0.67 - 1.08$ ). Let us note, however, that these two configurations are not stable [43].

In a similar way, we have also computed the impact of halo asphericity on the values of the  $J$  factors relevant for indirect searches of gamma-rays and neutrinos from DM annihilations and decays at the galactic center. We note that the variations with respect to the average value depend very weakly on the chosen ROI (around the galactic center). However, in these cases the variation with respect to the spherical averages are much smaller than those obtained for the local density. Including observational priors, for the case of DM annihilations and  $\langle\bar{J}_{\text{ann}}\rangle \simeq 590 \text{ (GeV/cm}^3)^2 \text{ kpc}$  (for a square ROI of  $3^{\circ} \times 3^{\circ}$  around the galactic center), the actual value of  $\bar{J}_{\text{ann}}$ , if the stellar disk coincides with the  $a - b$  plane of the DM halo, with a probability of 95%, lies in the interval (see upper right panel of Fig. 5)

$$\frac{\bar{J}_{\text{ann}}}{\langle\bar{J}_{\text{ann}}\rangle} = 0.95 - 1.09 , \quad (7.2)$$

whereas it is  $\bar{J}_{\text{ann}}/\langle\bar{J}_{\text{ann}}\rangle = 0.90 - 1.07$  ( $0.88 - 1.01$ ), if the stellar disk coincides with the  $a - c$  ( $b - c$ ) plane.

Including observational priors, for DM decays and  $\langle\bar{J}_{\text{dec}}\rangle \simeq 43$  ( $\text{GeV}/\text{cm}^3$ ) kpc (for the same ROI), the actual value of  $\bar{J}_{\text{dec}}$ , if the stellar disk coincides with the  $a - b$  plane of the DM halo, with a probability of 95%, lies in the interval (see upper right panel of Fig. 6)

$$\frac{\bar{J}_{\text{dec}}}{\langle\bar{J}_{\text{dec}}\rangle} = 0.93 - 1.13, \quad (7.3)$$

whereas it is  $\bar{J}_{\text{dec}}/\langle\bar{J}_{\text{dec}}\rangle = 0.82 - 1.12$  ( $0.83 - 1.04$ ), if the stellar disk coincides with the  $a - c$  ( $b - c$ ) plane.

The ranges above are quoted for values of the spherical averages equal to the  $J$  factors for a spherical NFW profile with  $r_s = 20$  kpc and  $\rho_{\odot} = 0.3$   $\text{GeV}/\text{cm}^3$  at  $R_{\odot} = 8.3$  kpc (for a square ROI of  $3^{\circ} \times 3^{\circ}$  around the galactic center), i.e.,  $\langle\bar{J}_{\text{ann}}\rangle \simeq 590$  ( $\text{GeV}/\text{cm}^3$ )<sup>2</sup> kpc and  $\langle\bar{J}_{\text{dec}}\rangle \simeq 43$  ( $\text{GeV}/\text{cm}^3$ ) kpc. However, it turns out that the corresponding values for other spherical DM profiles span a larger range than that owing to halo asphericity. For instance, for a Einasto profile [167] with the same local DM density and with  $\alpha = 0.17$ ,  $r_s = 20$  kpc,  $\langle\bar{J}_{\text{ann}}\rangle \simeq 10^3$  ( $\text{GeV}/\text{cm}^3$ )<sup>2</sup> kpc and  $\langle\bar{J}_{\text{dec}}\rangle \simeq 56$  ( $\text{GeV}/\text{cm}^3$ ) kpc. On the other hand, for a Burkert profile [168] with the same local DM density with  $r_s = 12$  kpc,  $\langle\bar{J}_{\text{ann}}\rangle \simeq 4.9$  ( $\text{GeV}/\text{cm}^3$ )<sup>2</sup> kpc and  $\langle\bar{J}_{\text{dec}}\rangle \simeq 11$  ( $\text{GeV}/\text{cm}^3$ ) kpc. Let us note that the less cuspy the DM profile the larger the variations of the  $J$  factors with respect to the spherical average [46], which can be understood in the same way  $\bar{J}_{\text{dec}}$  experiences larger variations than  $\bar{J}_{\text{ann}}$  for a given profile. Thus, we conclude that uncertainties originated from the non-sphericity of the Milky Way DM halo are smaller, and thus less important, than the uncertainties coming from the DM density profile.

In summary, we have quantified the systematic uncertainties on the local DM density and the  $J$  factors in a statistical way by using the results from the **Bolshoi** simulation. We note that halo asphericity could imply systematic errors on the local DM density at the level of current uncertainties, but in the case of the  $J$  factors they tend to be smaller than other errors. The determination of the DM density profile, not only is important for a better understanding of our galaxy, but also because they represent crucial parameters in direct and indirect DM searches. Hence, assessing their systematic uncertainties, and in particular due to halo asphericity, is of prime importance. Extracting DM properties from a positive signal or from a combination of positive signals will critically depend on the value of these parameters.

## Acknowledgments

We would like to thank Manuel Drees for useful discussions and comments. NB is supported by the São Paulo Research Foundation (FAPESP) under grants 2011/11973-4 and 2013/01792-8. JEF-R is supported by a FAPA starting grant from the Vicerrectoría de Investigaciones at Universidad de los Andes in Bogotá, Colombia. RG is supported by the DFG TRR33 ‘The Dark Universe’ and by the Helmholtz Alliance for Astroparticle Physics. SPR is supported by a Ramón y Cajal contract and by the Spanish MINECO under grant FPA2011-23596. SPR is also partially supported by PITN-GA-2011-289442-INVISIBLES and the Portuguese FCT through the projects CERN/FP/123580/2011, PTDC/FIS-NUC/0548/2012 and CFTEP-FCT Unit 777 (PEst-OE/FIS/UI0777/2013), which are partially funded through POCTI (FEDER).

## References

- [1] W. Dehnen and J. Binney, *Mass models of the Milky Way*, *Mon.Not.Roy.Astron.Soc.* **294** (1998) 429, [[astro-ph/9612059](#)].
- [2] A. Klypin, H. Zhao, and R. S. Somerville,  *$\Lambda$ CDM-based models for the Milky Way and M31 I: Dynamical models*, *Astrophys.J.* **573** (2002) 597–613, [[astro-ph/0110390](#)].
- [3] R. Catena and P. Ullio, *A novel determination of the local dark matter density*, *JCAP* **1008** (2010) 004, [[arXiv:0907.0018](#)].
- [4] M. Weber and W. de Boer, *Determination of the Local Dark Matter Density in our Galaxy*, *Astron.Astrophys.* **509** (2010) A25, [[arXiv:0910.4272](#)].
- [5] P. J. McMillan, *Mass models of the Milky Way*, *Mon.Not.Roy.Astron.Soc.* **414** (2011) 2446–2457, [[arXiv:1102.4340](#)].
- [6] F. Nesti and P. Salucci, *The Dark Matter halo of the Milky Way, AD 2013*, *JCAP* **1307** (2013) 016, [[arXiv:1304.5127](#)].
- [7] C. S. Frenk, S. D. White, M. Davis, and G. Efstathiou, *The formation of dark halos in a universe dominated by cold dark matter*, *Astrophys.J.* **327** (1988) 507–525.
- [8] N. Katz, *Dissipationless collapse in an expanding universe*, *Astrophys.J.* **368** (1991) 325–336.
- [9] J. Dubinski and R. Carlberg, *The Structure of cold dark matter halos*, *Astrophys.J.* **378** (1991) 496.
- [10] M. Warren, P. Quinn, J. Salmon, and W. Zurek, *Dark halos formed via dissipationless collapse: 1. shapes and alignment of angular momentum*, *Astrophys.J.* **399** (1992) 405.
- [11] J. Dubinski, *The Effect of dissipation on the shapes of dark halos*, *Astrophys.J.* **431** (1994) 617–624, [[astro-ph/9309001](#)].
- [12] Y. Jing and Y. Suto, *Triaxial modeling of halo density profiles with high-resolution N-body simulations*, *Astrophys.J.* **574** (2002) 538, [[astro-ph/0202064](#)].
- [13] S. Kasun and A. E. Evrard, *Shapes and alignments of galaxy cluster halos*, *Astrophys.J.* **629** (2005) 781–790, [[astro-ph/0408056](#)].
- [14] J. Bailin and M. Steinmetz, *Internal and external alignment of the shapes and angular momenta of  $\Lambda$ CDM halos*, *Astrophys.J.* **627** (2005) 647–665, [[astro-ph/0408163](#)].
- [15] P. F. Hopkins, N. Bahcall, and P. Bode, *Cluster alignments and ellipticities in  $\Lambda$ CDM cosmology*, *Astrophys.J.* **618** (2004) 1–15, [[astro-ph/0409652](#)].
- [16] B. Allgood et al., *The shape of dark matter halos: dependence on mass, redshift, radius, and formation*, *Mon.Not.Roy.Astron.Soc.* **367** (2006) 1781–1796, [[astro-ph/0508497](#)].
- [17] A. V. Macciò et al., *Concentration, Spin and Shape of Dark Matter Haloes: Scatter and the Dependence on Mass and Environment*, *Mon.Not.Roy.Astron.Soc.* **378** (2007) 55–71, [[astro-ph/0608157](#)].
- [18] P. Bett et al., *The spin and shape of dark matter haloes in the Millennium simulation of a  $\Lambda$ CDM universe*, *Mon.Not.Roy.Astron.Soc.* **376** (2007) 215–232, [[astro-ph/0608607](#)].
- [19] E. Hayashi, J. Navarro, and V. Springel, *The Shape of the Gravitational Potential in Cold Dark Matter Halos*, *Mon.Not.Roy.Astron.Soc.* **377** (2007) 50–62, [[astro-ph/0612327](#)].
- [20] M. Kuhlen, J. Diemand, and P. Madau, *The shapes, orientation, and alignment of Galactic dark matter subhalos*, *Astrophys.J.* **671** (2007) 1135–1146, [[arXiv:0705.2037](#)].
- [21] J. Stadel et al., *Quantifying the heart of darkness with GALLO - a multi-billion particle simulation of our galactic halo*, *Mon. Not. Roy. Astron. Soc.* **398** (2009) L21, [[arXiv:0808.2981](#)].

- [22] J. Muñoz Cuartas, A. Macciò, S. Gottlober, and A. Dutton, *The Redshift Evolution of  $\Lambda$ CDM Halo Parameters: Concentration, Spin, and Shape*, *Mon.Not.Roy.Astron.Soc.* **411** (2011) 584–594, [[arXiv:1007.0438](#)].
- [23] C. A. Vera-Ciro et al., *The Shape of Dark Matter Haloes in the Aquarius Simulations: Evolution and Memory*, *Mon.Not.Roy.Astron.Soc.* **416** (2011) 1377–1391, [[arXiv:1104.1566](#)].
- [24] M. D. Schneider, C. S. Frenk, and S. Cole, *The Shapes and Alignments of Dark Matter Halos*, *JCAP* **1205** (2012) 030, [[arXiv:1111.5616](#)].
- [25] C. Vera-Ciro, L. V. Sales, A. Helmi, and J. F. Navarro, *The shape of dark matter subhalos in the Aquarius simulations*, [arXiv:1402.0903](#).
- [26] S. Kazantzidis et al., *The Effect of gas cooling on the shapes of dark matter halos*, *Astrophys.J.* **611** (2004) L73–L76, [[astro-ph/0405189](#)].
- [27] J. Bailin et al., *Internal alignment of the halos of disk galaxies in cosmological hydrodynamic simulations*, *Astrophys.J.* **627** (2005) L17–L20, [[astro-ph/0505523](#)].
- [28] M. Gustafsson, M. Fairbairn, and J. Sommer-Larsen, *Baryonic Pinching of Galactic Dark Matter Haloes*, *Phys.Rev.* **D74** (2006) 123522, [[astro-ph/0608634](#)].
- [29] S. Kazantzidis, M. G. Abadi, and J. F. Navarro, *The Sphericalization of Dark Matter Halos by Galaxy Disks*, *Astrophys. J.* **720** (2010) L62, [[arXiv:1006.0537](#)].
- [30] S. Bryan et al., *The impact of baryons on the spins and shapes of dark matter haloes*, *Mon.Not.Roy.Astron.Soc.* **429** (2013) 3316–3329, [[arXiv:1207.4555](#)].
- [31] R. Olling and M. Merrifield, *Two measures of the shape of the milky way’s dark halo*, *Mon.Not.Roy.Astron.Soc.* **311** (2000) 361–369, [[astro-ph/9907353](#)].
- [32] R. Ibata, G. F. Lewis, M. Irwin, E. Totten, and T. R. Quinn, *Great circle tidal streams: evidence for a nearly spherical massive dark halo around the milky way*, *Astrophys.J.* **551** (2001) 294–311, [[astro-ph/0004011](#)].
- [33] A. Helmi, *Velocity trends in the debris of Sagittarius and the shape of the dark-matter halo of the galaxy*, *Astrophys.J.* **610** (2004) L97–L100, [[astro-ph/0406396](#)].
- [34] K. V. Johnston, D. R. Law, and S. R. Majewski, *A 2MASS all-sky view of the Sagittarius dwarf galaxy: 3. Constraints on the flattening of the Galactic halo*, *Astrophys.J.* **619** (2005) 800–806, [[astro-ph/0407565](#)].
- [35] D. R. Law, K. V. Johnston, and S. R. Majewski, *A 2MASS all-sky view of the Sagittarius dwarf galaxy. 4. Modeling the Sagittarius tidal tails*, *Astrophys.J.* **619** (2005) 807–823, [[astro-ph/0407566](#)].
- [36] M. Fellhauer et al., *The origin of the bifurcation in the Sagittarius stream*, *Astrophys.J.* **651** (2006) 167–173, [[astro-ph/0605026](#)].
- [37] D. Martínez-Delgado, J. Peñarrubia, M. Jurić, E. J. Alfaro, and Z. Ivezić, *The Virgo stellar over-density: Mapping the infall of the Sagittarius tidal stream onto the Milky Way disk*, *Astrophys.J.* **660** (2007) 1264–1272, [[astro-ph/0609104](#)].
- [38] D. R. Law, S. R. Majewski, and K. V. Johnston, *Evidence for a Triaxial Milky Way Dark Matter Halo from the Sagittarius Stellar Tidal Stream*, *Astrophys.J.* **703** (2009) L67–L71, [[arXiv:0908.3187](#)].
- [39] D. R. Law and S. R. Majewski, *The Sagittarius Dwarf Galaxy: a Model for Evolution in a Triaxial Milky Way Halo*, *Astrophys.J.* **714** (2010) 229–254, [[arXiv:1003.1132](#)].
- [40] N. Deg and L. Widrow, *The Sagittarius Stream and Halo Triaxiality*, *Mon.Not.Roy.Astron.Soc.* **428** (2013) 912–922, [[arXiv:1209.6614](#)].



- [41] R. Ibata, G. F. Lewis, N. F. Martin, M. Bellazzini, and M. Correnti, *Does the Sagittarius Stream constrain the Milky Way halo to be triaxial?*, *Astrophys.J.* **765** (2013) L15, [[arXiv:1212.4958](#)].
- [42] C. Vera-Ciro and A. Helmi, *Constraints on the shape of the Milky Way dark matter halo from the Sagittarius stream*, *Astrophys.J.* **773** (2013) L4, [[arXiv:1304.4646](#)].
- [43] V. P. Debattista et al., *What's Up in the Milky Way? The Orientation of the Disc Relative to the Triaxial Halo*, *Mon.Not.Roy.Astron.Soc.* **434** (2013) 2971–2981, [[arXiv:1301.2670](#)].
- [44] M. Zemp et al., *The Graininess of Dark Matter Haloes*, *Mon.Not.Roy.Astron.Soc.* **394** (2009) 641–659, [[arXiv:0812.2033](#)].
- [45] M. Pato, O. Agertz, G. Bertone, B. Moore, and R. Teyssier, *Systematic uncertainties in the determination of the local dark matter density*, *Phys.Rev.* **D82** (2010) 023531, [[arXiv:1006.1322](#)].
- [46] E. Athanassoula, F.-S. Ling, and E. Nezri, *Halo geometry and dark matter annihilation signal*, *Phys.Rev.* **D72** (2005) 083503, [[astro-ph/0504631](#)].
- [47] A. Klypin, S. Trujillo-Gómez, and J. Primack, *Halos and galaxies in the standard cosmological model: results from the Bolshoi simulation*, *Astrophys.J.* **740** (2011) 102, [[arXiv:1002.3660](#)].
- [48] G. Bertone, D. Hooper, and J. Silk, *Particle dark matter: Evidence, candidates and constraints*, *Phys.Rept.* **405** (2005) 279–390, [[hep-ph/0404175](#)].
- [49] J. A. R. Caldwell and J. P. Ostriker, *The Mass distribution within our Galaxy: A Three component model*, *Astrophys. J.* **251** (1981) 61.
- [50] J. N. Bahcall, *The distribution of stars perpendicular to a galactic disk*, *Astrophys.J.* **276** (1984) 156–168.
- [51] K. Kuijken and G. Gilmore, *The mass distribution in the galactic disc - Part I - A technique to determine the integral surface mass density of the disc near the Sun*, *Mon.Not.Roy.Astron.Soc.* **239** (1989) 571–603.
- [52] K. Kuijken and G. Gilmore, *The Mass Distribution in the Galactic Disc - Part II - Determination of the Surface Mass Density of the Galactic Disc Near the Sun*, *Mon.Not.Roy.Astron.Soc.* **239** (1989) 605–649.
- [53] J. N. Bahcall, C. Flynn, and A. Gould, *Local dark matter from a carefully selected sample*, *Astrophys.J.* **389** (1992) 234–250.
- [54] L. E. Strigari and R. Trotta, *Reconstructing WIMP Properties in Direct Detection Experiments Including Galactic Dark Matter Distribution Uncertainties*, *JCAP* **0911** (2009) 019, [[arXiv:0906.5361](#)].
- [55] W. de Boer and M. Weber, *The Dark Matter Density in the Solar Neighborhood reconsidered*, *JCAP* **1104** (2011) 002, [[arXiv:1011.6323](#)].
- [56] F. Iocco, M. Pato, G. Bertone, and P. Jetzer, *Dark Matter distribution in the Milky Way: microlensing and dynamical constraints*, *JCAP* **1111** (2011) 029, [[arXiv:1107.5810](#)].
- [57] P. Salucci, F. Nesti, G. Gentile, and C. F. Martins, *The dark matter density at the Sun's location*, *Astron. Astrophys.* **523** (2010) A83, [[arXiv:1003.3101](#)].
- [58] J. Holmberg and C. Flynn, *The local density of matter mapped by Hipparcos*, *Mon.Not.Roy.Astron.Soc.* **313** (2000) 209–216, [[astro-ph/9812404](#)].
- [59] J. Holmberg and C. Flynn, *The Local surface density of disc matter mapped by Hipparcos*, *Mon.Not.Roy.Astron.Soc.* **352** (2004) 440, [[astro-ph/0405155](#)].
- [60] J. Bovy and S. Tremaine, *On the local dark matter density*, *Astrophys.J.* **756** (2012) 89, [[arXiv:1205.4033](#)].



- [61] L. Zhang et al., *The Gravitational Potential Near the Sun From SEGUE K-dwarf Kinematics*, *Astrophys.J.* **772** (2013) 108, [[arXiv:1209.0256](#)].
- [62] J. Bovy and H.-W. Rix, *A Direct Dynamical Measurement of the Milky Way’s Disk Surface Density Profile, Disk Scale Length, and Dark Matter Profile at  $4 \text{ kpc} \lesssim R \lesssim 9 \text{ kpc}$* , *Astrophys.J.* **779** (2013) 115, [[arXiv:1309.0809](#)].
- [63] S. Garbari, J. I. Read, and G. Lake, *Limits on the local dark matter density*, *Mon.Not.Roy.Astron.Soc.* **416** (2011) 2318–2340, [[arXiv:1105.6339](#)].
- [64] S. Garbari, C. Liu, J. I. Read, and G. Lake, *A new determination of the local dark matter density from the kinematics of K dwarfs*, *Mon.Not.Roy.Astron.Soc.* **425** (2012) 1445, [[arXiv:1206.0015](#)].
- [65] J. Read, *The Local Dark Matter Density*, *J.Phys.* **G41** (2014) 063101, [[arXiv:1404.1938](#)].
- [66] L. Bergström, P. Ullio, and J. H. Buckley, *Observability of gamma-rays from dark matter neutralino annihilations in the Milky Way halo*, *Astropart.Phys.* **9** (1998) 137–162, [[astro-ph/9712318](#)].
- [67] M. Weber, *Determination of the Dark Matter profile from the EGRET excess of diffuse Galactic gamma radiation*, [[arXiv:0710.5119](#)].
- [68] S. Dodelson, D. Hooper, and P. D. Serpico, *Extracting the Gamma Ray Signal from Dark Matter Annihilation in the Galactic Center Region*, *Phys. Rev.* **D77** (2008) 063512, [[arXiv:0711.4621](#)].
- [69] N. Bernal and S. Palomares-Ruiz, *Constraining Dark Matter Properties with Gamma-Rays from the Galactic Center with Fermi-LAT*, [[arXiv:1006.0477](#)].
- [70] D. Hooper and L. Goodenough, *Dark Matter Annihilation in The Galactic Center As Seen by the Fermi Gamma Ray Space Telescope*, *Phys.Lett.* **B697** (2011) 412–428, [[arXiv:1010.2752](#)].
- [71] N. Bernal, *Reconstructing Dark Matter Properties via Gamma-Rays with Fermi-LAT*, *PoS IDM2010* (2011) 022, [[arXiv:1012.0217](#)].
- [72] N. Bernal and S. Palomares-Ruiz, *Constraining the Milky Way Dark Matter Density Profile with Gamma-Rays with Fermi-LAT*, *JCAP* **1201** (2012) 006, [[arXiv:1103.2377](#)].
- [73] T.-S. Lu, T.-K. Dong, and J. Wu, *The spatial distribution of dark matter annihilation originating from a gamma-ray line signal*, *Res.Astron.Astrophys.* **14** (2014) 520–526, [[arXiv:1312.0357](#)].
- [74] T. Daylan et al., *The Characterization of the Gamma-Ray Signal from the Central Milky Way: A Compelling Case for Annihilating Dark Matter*, [[arXiv:1402.6703](#)].
- [75] K. Riebe et al., *The MultiDark Database: Release of the Bolshoi and MultiDark Cosmological Simulations*, *Astronomische Nachrichten* (2013) 691–708, [[arXiv:1109.0003](#)].
- [76] A. V. Kravtsov, A. A. Klypin, and A. M. Khokhlov, *Adaptive refinement tree: A New high resolution N body code for cosmological simulations*, *Astrophys.J.Suppl.* **111** (1997) 73, [[astro-ph/9701195](#)].
- [77] **WMAP** Collaboration, G. Hinshaw et al., *Nine-Year Wilkinson Microwave Anisotropy Probe (WMAP) Observations: Cosmological Parameter Results*, *Astrophys.J.Suppl.* **208** (2013) 19, [[arXiv:1212.5226](#)].
- [78] A. Klypin and J. Holtzman, *Particle mesh code for cosmological simulations*, [[astro-ph/9712217](#)].
- [79] G. Bryan and M. Norman, *Statistical properties of x-ray clusters: Analytic and numerical comparisons*, *Astrophys.J.* **495** (1998) 80, [[astro-ph/9710107](#)].
- [80] M. Zemp, O. Y. Gnedin, N. Y. Gnedin, and A. V. Kravtsov, *On determining the shape of matter distributions*, *Astrophys.J.Suppl.* **197** (2011) 30, [[arXiv:1107.5582](#)].

- [81] J. F. Navarro, C. S. Frenk, and S. D. White, *The Structure of cold dark matter halos*, *Astrophys.J.* **462** (1996) 563–575, [[astro-ph/9508025](#)].
- [82] J. F. Navarro, C. S. Frenk, and S. D. White, *A Universal density profile from hierarchical clustering*, *Astrophys.J.* **490** (1997) 493–508, [[astro-ph/9611107](#)].
- [83] F. Prada, A. A. Klypin, A. J. Cuesta, J. E. Betancort-Rijo, and J. Primack, *Halo concentrations in the standard  $\Lambda$ CDM cosmology*, *Mon.Not.Roy.Astron.Soc.* **423** (2012) 3018–3030, [[arXiv:1104.5130](#)].
- [84] M. Meneghetti and E. Rasia, *Reconciling extremely different concentration-mass relations*, [[arXiv:1303.6158](#)].
- [85] M. Franx, G. Illingworth, and T. de Zeeuw, *The ordered nature of elliptical galaxies - Implications for their intrinsic angular momenta and shapes*, *Astrophys.J.* **383** (1991) 112–134.
- [86] A. Knebe and V. Wiessner, *Triaxial vs. Spherical Dark Matter Halo Profiles*, *Publ.Astron.Soc.Austral.* **23** (2006) 125–128, [[astro-ph/0609361](#)].
- [87] N. Deg and L. Widrow, *Incorporating Streams into Milky Way Models*, *Mon.Not.Roy.Astron.Soc.* **439** (2014) 2678, [[arXiv:1401.4070](#)].
- [88] M. C. Smith et al., *The RAVE Survey: Constraining the Local Galactic Escape Speed*, *Mon.Not.Roy.Astron.Soc.* **379** (2007) 755–772, [[astro-ph/0611671](#)].
- [89] SDSS Collaboration, X. Xue et al., *The Milky Way’s Circular Velocity Curve to 60 kpc and an Estimate of the Dark Matter Halo Mass from Kinematics of 2400 SDSS Blue Horizontal Branch Stars*, *Astrophys.J.* **684** (2008) 1143–1158, [[arXiv:0801.1232](#)].
- [90] A. Deason et al., *The cold veil of the Milky Way stellar halo*, *Mon.Not.Roy.Astron.Soc.* **425** (2012) 2840–2853, [[arXiv:1205.6203](#)].
- [91] J. Bovy et al., *The Milky Way’s circular velocity curve between 4 and 14 kpc from APOGEE data*, *Astrophys.J.* **759** (2012) 131, [[arXiv:1209.0759](#)].
- [92] P. R. Kafle, S. Sharma, G. F. Lewis, and J. Bland-Hawthorn, *Kinematics of the stellar halo and the mass distribution of the Milky Way using BHB stars*, *Astrophys.J.* **761** (2012) 98, [[arXiv:1210.7527](#)].
- [93] C. S. Kochanek, *The Mass of the Milky Way galaxy*, *Astrophys.J.* **457** (1996) 228, [[astro-ph/9505068](#)].
- [94] M. Wilkinson and N. Evans, *The present and future mass of the Milky Way halo*, *Mon.Not.Roy.Astron.Soc.* **310** (1999) 645, [[astro-ph/9906197](#)].
- [95] Y.-S. Li and S. D. White, *Masses for the Local Group and the Milky Way*, *Mon.Not.Roy.Astron.Soc.* **384** (2008) 1459–1468, [[arXiv:0710.3740](#)].
- [96] L. Watkins, N. Evans, and J. An, *The Masses of the Milky Way and Andromeda galaxies*, *Mon.Not.Roy.Astron.Soc.* **406** (2010) 264, [[arXiv:1002.4565](#)].
- [97] M. Boylan-Kolchin, G. Besla, and L. Hernquist, *Dynamics of the Magellanic Clouds in a  $\Lambda$ CDM Universe*, *Mon.Not.Roy.Astron.Soc.* **414** (2011) 1560, [[arXiv:1010.4797](#)].
- [98] M. T. Busha, P. J. Marshall, R. H. Wechsler, A. Klypin, and J. Primack, *The Mass Distribution and Assembly of the Milky Way from the Properties of the Magellanic Clouds*, *Astrophys.J.* **743** (2011) 40, [[arXiv:1011.2203](#)].
- [99] S. T. Sohn et al., *The Space Motion of Leo I: Hubble Space Telescope Proper Motion and Implied Orbit*, *Astrophys.J.* **768** (2013) 139, [[arXiv:1210.6039](#)].
- [100] M. Boylan-Kolchin, J. S. Bullock, S. T. Sohn, G. Besla, and R. P. van der Marel, *The Space Motion of Leo I: The Mass of the Milky Way’s Dark Matter Halo*, *Astrophys. J.* **768** (2013) 140, [[arXiv:1210.6046](#)].

- [101] N. Kallivayalil, G. Besla, R. Sanderson, and C. Alcock, *Revisiting the Role of M31 in the Dynamical History of the Magellanic Clouds*, *Astrophys.J.* **700** (2009) 924–930, [[arXiv:0905.4283](#)].
- [102] O. Y. Gnedin, W. R. Brown, M. J. Geller, and S. J. Kenyon, *The Mass Profile of the Galaxy to 80 kpc*, *Astrophys.J.* **720** (2010) L108, [[arXiv:1005.2619](#)].
- [103] N. Przybilla, A. Tillich, U. Heber, and R.-D. Scholz, *Weighing the Galactic dark matter halo: a lower mass limit from the fastest halo star known*, *Astrophys.J.* **718** (2010) 37–42, [[arXiv:1005.5026](#)].
- [104] S. Samurović and A. Lalović, *The Jeans modeling of the Milky Way galaxy: implications of the kinematics of the stellar halo*, *Astron.Astrophys.* **531** (2011) A82.
- [105] C. A. Vera-Ciro, A. Helmi, E. Starkeburg, and M. A. Breddels, *Not too big, not too small: the dark halos of the dwarf spheroidals in the Milky Way*, *Mon.Not.Roy.Astron.Soc.* **428** (2013) 1696–1703, [[arXiv:1202.6061](#)].
- [106] T. Piffl et al., *The RAVE survey: the Galactic escape speed and the mass of the Milky Way*, *Astron.Astrophys.* **562** (2014) A91, [[arXiv:1309.4293](#)].
- [107] T. Sakamoto, M. Chiba, and T. C. Beers, *The Mass of the Milky Way: Limits from a newly assembled set of halo objects*, *Astron.Astrophys.* **397** (2003) 899–912, [[astro-ph/0210508](#)].
- [108] G. Battaglia et al., *The Radial velocity dispersion profile of the Galactic Halo: Constraining the density profile of the dark halo of the Milky Way*, *Mon.Not.Roy.Astron.Soc.* **364** (2005) 433–442, [[astro-ph/0506102](#)].
- [109] W. Dehnen, D. McLaughlin, and J. Sachania, *The velocity dispersion and mass profile of the milky way*, *Mon.Not.Roy.Astron.Soc.* **369** (2006) 1688–1692, [[astro-ph/0603825](#)].
- [110] Y. Sofue, M. Honma, and T. Omodaka, *Unified Rotation Curve of the Galaxy – Decomposition into de Vaucouleurs Bulge, Disk, Dark Halo, and the 9-kpc Rotation Dip –*, *PASJ* **61** (2009) 227, [[arXiv:0811.0859](#)].
- [111] Y. Sofue, *Pseudo Rotation Curve connecting the Galaxy, Dark Halo, and Local Group*, *PASJ* **61** (2009) 153, [[arXiv:0811.0860](#)].
- [112] Y. Sofue, *A Grand Rotation Curve and Dark Matter Halo in the Milky Way Galaxy*, *PASJ* **64** (2012) 75, [[arXiv:1110.4431](#)].
- [113] P. Bhattacharjee, S. Chaudhury, and S. Kundu, *Rotation Curve of the Milky Way out to  $\sim 200$  kpc*, *Astrophys.J.* **785** (2014) 63, [[arXiv:1310.2659](#)].
- [114] A. A. Dutton, C. Conroy, F. C. d. Bosch, F. Prada, and S. More, *The Kinematic Connection Between Galaxies and Dark Matter Haloes*, *Mon.Not.Roy.Astron.Soc.* **407** (2010) 2–16, [[arXiv:1004.4626](#)].
- [115] R. Reyes, R. Mandelbaum, J. Gunn, J. Pizagno, and C. Lackner, *Calibrated Tully-Fisher relations for improved estimates of disk rotation velocities*, *Mon.Not.Roy.Astron.Soc.* **417** (2011) 2347–2386, [[arXiv:1106.1650](#)].
- [116] Q. Guo, S. White, C. Li, and M. Boylan-Kolchin, *How do galaxies populate Dark Matter halos?*, *Mon.Not.Roy.Astron.Soc.* **404** (2010) 1111, [[arXiv:0909.4305](#)].
- [117] R. M. Reddick, R. H. Wechsler, J. L. Tinker, and P. S. Behroozi, *The Connection between Galaxies and Dark Matter Structures in the Local Universe*, *Astrophys.J.* **771** (2013) 30, [[arXiv:1207.2160](#)].
- [118] B. P. Moster, T. Naab, and S. D. White, *Galactic star formation and accretion histories from matching galaxies to dark matter haloes*, *Mon.Not.Roy.Astron.Soc.* **428** (2013) 3121–3138, [[arXiv:1205.5807](#)].

- [119] O. Gerhard, *Mass distribution in our Galaxy*, *Space Sci.Rev.* **100** (2002) 129–138, [[astro-ph/0203110](#)].
- [120] C. Flynn, J. Holmberg, L. Portinari, B. Fuchs, and H. Jahreiss, *On the mass-to-light ratio of the local Galactic disc and the optical luminosity of the Galaxy*, *Mon.Not.Roy.Astron.Soc.* **372** (2006) 1149–1160, [[astro-ph/0608193](#)].
- [121] K. Kuijken and G. Gilmore, *The galactic disk surface mass density and the Galactic force  $K(z)$  at  $Z = 1.1$  kiloparsecs*, *Astrophys.J.* **367** (1991) L9–L13.
- [122] A. Siebert, O. Bienayme, and C. Soubiran, *Vertical distribution of Galactic disk stars : 2. The Surface mass density in the Galactic plane*, *Astron.Astrophys.* **399** (2003) 531–542, [[astro-ph/0211328](#)].
- [123] V. Korchagin, T. M. Girard, T. Borkova, D. Dinescu, and W. F. van Altena, *Local surface density of the Galactic disk from a 3-D stellar velocity sample*, *Astron.J.* **126** (2003) 2896, [[astro-ph/0308276](#)].
- [124] O. Bienayme, C. Soubiran, T. Mishenina, V. Kovtyukh, and A. Siebert, *Vertical distribution of galactic disk stars. 3. the galactic disk surface mass density from red clump giants*, *Astron.Astrophys.* **446** (2005) 933, [[astro-ph/0510431](#)].
- [125] K. Kuijken and G. Gilmore, *The Mass Distribution in the Galactic Disc - Part III - the Local Volume Mass Density*, *Mon.Not.Roy.Astron.Soc.* **239** (1989) 651–664.
- [126] C. Flynn and B. Fuchs, *Density of dark matter in the Galactic disk*, *Mon.Not.Roy.Astron.Soc.* **270** (1994) 471.
- [127] A. Gould, J. N. Bahcall, and C. Flynn, *Disk  $M$  dwarf luminosity function from HST star counts*, *Astrophys.J.* **465** (1996) 759, [[astro-ph/9505087](#)].
- [128] Z. Zheng, C. Flynn, A. Gould, J. N. Bahcall, and S. Salim,  *$M$  dwarfs from Hubble Space Telescope star counts. 4*, *Astrophys.J.* **555** (2001) 393–404, [[astro-ph/0102442](#)].
- [129] J. Binney and N. Evans, *Cuspy dark-matter haloes and the Galaxy*, *Mon.Not.Roy.Astron.Soc.* **327** (2001) L27, [[astro-ph/0108505](#)].
- [130] J. Bovy, H.-W. Rix, and D. W. Hogg, *The Milky Way has no thick disk*, *Astrophys.J.* **751** (2012) 131, [[arXiv:1111.6585](#)].
- [131] R. Olling and M. Merrifield, *Luminous and dark matter in the milky way*, *Mon.Not.Roy.Astron.Soc.* **326** (2001) 164, [[astro-ph/0104465](#)].
- [132] F. J. Kerr and D. Lynden-Bell, *Review of galactic constants*, *Mon. Not. Roy. Astron. Soc.* **221** (1986) 1023.
- [133] M. J. Reid, *The distance to the center of the galaxy*, *Ann. Rev. Astron. Astrophys.* **31** (1993) 345.
- [134] I. Nikiforov, *The Distance to the Center of the Galaxy: the Current State-of-the-Art in Measuring  $R_0$* , in *Order and Chaos in Stellar and Planetary Systems* (G. G. Byrd, K. V. Kholshevnikov, A. A. Myllri, I. I. Nikiforov, and V. V. Orlov, eds.), vol. 316 of *Astronomical Society of the Pacific Conference Series*, p. 199, 2004.
- [135] V. S. Avedisova, *The galactic constants and rotation curve from molecular-gas observations*, *Astron. Rept.* **49** (2005) 435.
- [136] C. Francis and E. Anderson, *Two estimates of the distance to the Galactic centre*, [[arXiv:1309.2629](#)].
- [137] E. Bica, C. Bonatto, B. Barbuy, and S. Ortolani, *Globular cluster system and Milky Way properties revisited*, *Astron. Astrophys.* **450** (2006) 105, [[astro-ph/0511788](#)].

- [138] M. J. Collinge, T. Sumi, and D. Fabrycky, *Catalog of fundamental mode rr lyrae stars in the galactic bulge from the optical gravitational lensing experiment*, *Astrophys.J.* **651** (2006) 197–210, [[astro-ph/0601137](#)].
- [139] S. Nishiyama et al., *The Distance to the Galactic Center Derived From Infrared Photometry of Bulge Red Clump Stars*, *Astrophys.J.* **647** (2006) 1093–1098, [[astro-ph/0607408](#)].
- [140] M. Groenewegen, A. Udalski, and G. Bono, *The distance to the Galactic Centre based on Population-II Cepheids and RR Lyrae stars*, *Astron.Astrophys.* **481** (2008) 441–448, [[arXiv:0801.2652](#)].
- [141] M. W. Feast, C. D. Laney, T. D. Kinman, F. van Leeuwen, and P. A. Whitelock, *The Luminosities and Distance Scales of Type II Cepheid and RR Lyrae variables*, *Mon. Not. Roy. Astron. Soc.* **386** (2008) 2115–2134, [[arXiv:0803.0466](#)].
- [142] A. Kunder and B. Chaboyer, *Metallicity Analysis of MACHO Galactic Bulge RR0 Lyrae stars from their Lightcurves*, *Astrophys. J.* **136** (2008) 2441, [[arXiv:0809.1645](#)].
- [143] E. Vanhollebeke, M. A. T. Groenewegen, and L. Girardi, *Stellar populations in the Galactic bulge. Modelling the Galactic bulge with TRILEGAL*, *Astron. Astrophys.* **498** (2009) 95, [[arXiv:0903.0946](#)].
- [144] D. J. Majaess, D. G. Turner, and D. J. Lane, *Characteristics of the Galaxy according to Cepheids*, *Mon.Not.Roy.Astron.Soc.* **398** (2009) 263–270, [[arXiv:0903.4206](#)].
- [145] A. K. Dambis, *The kinematics and zero-point of the logP - <MK> relation for Galactic RR Lyrae variables via statistical parallax*, *Mon.Not.Roy.Astron.Soc.* **396** (2009) 553–569.
- [146] N. Matsunaga et al., *A near-infrared survey of Miras and the distance to the Galactic Centre*, *Mon.Not.Roy.Astron.Soc.* **399** (2009) 1709–1729, [[arXiv:0907.2761](#)].
- [147] D. J. Majaess, *Concerning the Distance to the Center of the Milky Way and its Structure*, *Acta Astron.* **60** (2010) 55, [[arXiv:1002.2743](#)].
- [148] P. Pietrukowicz et al., *The Optical Gravitational Lensing Experiment. Analysis of the bulge RR Lyrae population from the OGLE-III data*, *Astrophys.J.* **750** (2012) 169, [[arXiv:1107.3152](#)].
- [149] D. M. Nataf et al., *Reddening and Extinction Toward the Galactic Bulge from OGLE-III: The Inner Milky Way's  $R_V = 2.5$  Extinction Curve*, *Astrophys.J.* **769** (2013) 88, [[arXiv:1208.1263](#)].
- [150] N. Matsunaga et al., *Cepheids and other short-period variables near the Galactic Centre*, *Mon. Not. Roy. Astron. Soc.* **429** (2013) 385–397, [[arXiv:1211.0151](#)].
- [151] K. Ando et al., *Astrometry of Galactic Star-Forming Region ON2N with VERA: Estimation of the Galactic Constants*, *PASJ* **63** (2011) 45–51.
- [152] Y. Sofue, T. Nagayama, M. Matsui, and A. Nakagawa, *Near-Solar-Circle Method for Determination of the Galactic Constants*, *PASJ* **63** (2011) 867–871, [[arXiv:1105.1219](#)].
- [153] V. Bobylev, *Estimation of the SolarGalactocentric Distance and Rotation Velocity from Near-Solar-Circle Objects*, *Astron.Lett.* **39** (2013) 95–103, [[arXiv:1212.6616](#)].
- [154] M. Sato, M. Reid, A. Brunthaler, and K. Menten, *Trigonometric Parallax of W51 Main/South*, *Astrophys.J.* **720** (2010) 1055–1065, [[arXiv:1006.4218](#)].
- [155] R. Schonrich, *Galactic Rotation and Solar Motion from Stellar Kinematics*, *Mon. Not. Roy. Astron. Soc.* **427** (2012) 274–287, [[arXiv:1207.3079](#)].
- [156] M. Reid, K. Menten, X. Zheng, A. Brunthaler, and Y. Xu, *A Trigonometric Parallax of Sgr B2*, *Astrophys.J.* **705** (2009) 1548–1553, [[arXiv:0908.3637](#)].
- [157] M. J. Reid et al., *Trigonometric Parallaxes of Massive Star Forming Regions: VI. Galactic Structure, Fundamental Parameters and Non- Circular Motions*, *Astrophys. J.* **700** (2009) 137, [[arXiv:0902.3913](#)].



- [158] P. J. McMillan and J. J. Binney, *The uncertainty in Galactic parameters*, *Mon. Not. Roy. Astron. Soc.* **402** (2010) 934, [[arXiv:0907.4685](#)].
- [159] J. Bovy, D. W. Hogg, and H.-W. Rix, *Galactic masers and the Milky Way circular velocity*, *Astrophys. J.* **704** (2009) 1704, [[arXiv:0907.5423](#)].
- [160] M. Honma et al., *Fundamental Parameters of the Milky Way Galaxy Based on VLBI astrometry*, *PASJ* **64** (2012) 136, [[arXiv:1211.3843](#)].
- [161] R. Schoenrich, J. Binney, and W. Dehnen, *Local Kinematics and the Local Standard of Rest*, *Mon. Not. Roy. Astron. Soc.* **403** (2010) 1829–1833, [[arXiv:0912.3693](#)].
- [162] M. Reid et al., *Trigonometric Parallaxes of High Mass Star Forming Regions: the Structure and Kinematics of the Milky Way*, *Astrophys. J.* **783** (2014) 130, [[arXiv:1401.5377](#)].
- [163] A. M. Ghez et al., *Measuring Distance and Properties of the Milky Way’s Central Supermassive Black Hole with Stellar Orbits*, *Astrophys. J.* **689** (2008) 1044, [[arXiv:0808.2870](#)].
- [164] S. Gillessen et al., *Monitoring stellar orbits around the Massive Black Hole in the Galactic Center*, *Astrophys. J.* **692** (2009) 1075, [[arXiv:0810.4674](#)].
- [165] S. Gillessen et al., *The orbit of the star S2 around SgrA\* from VLT and Keck data*, *Astrophys. J.* **707** (2009) L114–L117, [[arXiv:0910.3069](#)].
- [166] T. Do et al., *Three-dimensional Stellar Kinematics at the Galactic Center: Measuring the Nuclear Star Cluster Spatial Density Profile, Black Hole Mass, and Distance*, *Astrophys. J. Letters* **779** (2013) L6, [[arXiv:1311.0886](#)].
- [167] J. Einasto, *On the Construction of a Composite Model for the Galaxy and on the Determination of the System of Galactic Parameters*, *Trudy Inst. Astrofiz. Alma-Ata* **51** (1965) 87.
- [168] A. Burkert, *The Structure of dark matter halos in dwarf galaxies*, *IAU Symp.* **171** (1996) 175, [[astro-ph/9504041](#)].